



Evaluation of Static Line Webbing Materials Subjected to Simulated Airdrop Operating Conditions

by Robert B. Dooley, Robert P. Kaste, James M. Sands,
Gary W. Thibault, and William L. Millette

ARL-TR-2713

April 2002

Approved for public release; distribution is unlimited.

20020702 110

The findings in this report are not to be construed as an official Department of the Army position unless so designated by other authorized documents.

Citation of manufacturer's or trade names does not constitute an official endorsement or approval of the use thereof.

Destroy this report when it is no longer needed. Do not return it to the originator.

Army Research Laboratory

Aberdeen Proving Ground, MD 21005-5069

ARL-TR-2713

April 2002

Evaluation of Static Line Webbing Materials Subjected to Simulated Airdrop Operating Conditions

Robert B. Dooley, Robert P. Kaste,
and James M. Sands

Weapons and Materials Research Directorate, ARL

Gary W. Thibault and William L. Millette

U.S. Army Soldier Biological and Chemical Command, Natick Soldier Center

Abstract

An investigation was conducted to evaluate the mechanical performance of two types of static line webbing materials. Conventional Type VIII static line webbing and a proposed replacement, referred to as AbsorbEdge, were the primary subjects of the investigation.

Tests were performed to evaluate the effect of each identified and simulated airdrop operating condition. Test methods used in the investigation included straight and 90° bend tensile tests to evaluate the effects of straining over a series of specified bend radii. Additional tests were performed to investigate the effect of textured bend surfaces, the number of twists in a line between test grips, the effect of retained water in the line, the effect of mechanical fatigue, and the effect of various cotton and polymer-based textile sheaths located at the bend fixture/specimen interface.

Results from these and other tests are contrasted against the results of straight-pull tests to evaluate the adverse effect of the test variables on the baseline strength of each material. A theory regarding how the line construction distributes tensile loads around a door edge and decays line system strength is presented. Test results are used to compliment failure observations and are presented within this report.

Acknowledgments

The authors of this report would like to acknowledge the following individuals for their assistance in this research effort:

- Paul Moy for providing laboratory facilities and data acquisition equipment required to perform the experiments,
- Gary Sprenkle, Keith Dougherty, James Leonard, Harry Baker, and Thomas Puckett for the fabrication of the test fixtures,
- Panagiotis Blanas for his insightful comments regarding nondestructive testing techniques for inexpensive “in-the-field” inspections,
- Jim Stauffer and Brad Lewis of the U.S. Aberdeen Test Center for their high-speed video documentation efforts, and
- José A. Milette of the U.S. Army Soldier Biological and Chemical Command, Natick Soldier Center, for providing funding and guidance in collaboration with senior engineers and coauthors at that agency.

INTENTIONALLY LEFT BLANK.

Contents

Acknowledgments	iii
List of Figures	vii
List of Tables	xi
1. Introduction	1
2. Characterization of Failed Static Line Material	4
3. Assessment of DSC Results	9
4. Tensile Testing of Static Line Webbing Material	9
5. 90° Bend Testing Procedure	10
6. Tensile Test Results	12
6.1 Performance of T-VIII and AbsorbEdge Webbing in Straight, Bent, and Cotton-Sheathed Test Configurations	12
6.2 Teflon, Nylon, and Kevlar Sheath Tests.....	19
6.3 Effect of Twists in a Static Line.....	20
6.4 Effect of Retained Water Tests.....	20
6.5 Preconditioned Static Line Tests	23
6.6 High-Speed Video Observation of Rupture Events	25
7. Web Construction and Failure Characteristics	27
8. Validation of Uneven Web Translations	36
9. Test Data Summary	39
10. Conclusions and Recommendations for Future Work	42

11. References	47
Appendix A. Bend Testing Fixture	49
Appendix B. Typical Results Data	61
Distribution List	63
Report Documentation Page	81

List of Figures

Figure 1. Basic components of the T-VIII static line system [2].	2
Figure 2. Onboard view of a static line extending out of an aircraft door in the postjump, preparachute deployment configuration.	3
Figure 3. DSC investigation of two field failed nylon jump cords demonstrating the effective use of thermal characterization for discerning compositional differences in the two materials. Assignment of each of the polymer fibers is shown in the legend.	5
Figure 4. DSC trace of nylon 6 from room temperature through the crystalline melting point of nylon ropes. Agreement between results measured in and far from the failure zone for a single rope is excellent.	6
Figure 5. Crystalline melting traces of fielded nylon 6 jump cords determined using DSC. Fielded samples show no substantive variations between bulk matrix fibers attained far from the failure zone and fibers extracted from the failure zone.	7
Figure 6. DSC trace of nylon 6,6 from room temperature through the crystalline melting point of nylon ropes. Agreement between various samples is excellent.	7
Figure 7. Crystalline melting region for nylon 6,6-based jump cords showing minimal deviations in crystalline structures for factory original vs. field failed cords.	8
Figure 8. The 90° bend fixture loaded with a static line specimen at ~2000 lb.	11
Figure 9. The 90° bend fixture (a) loaded with a static line (note the green pen marks on the specimen indicating the original position of contact with the bend plate and the position of the lines relative to the split in the grip) and (b) unloaded with the lower grip in the open position.	11
Figure 10. Test results extracted from Table 2 showing trends of strength as a function of bend plate diameter and texture both with and without cotton sheathing.	14
Figure 11. Strength reduction as a function of smooth bend plate diameter.	15
Figure 12. Strength of static lines tested with rough bend plate diameter.	16
Figure 13. Strength loss as a function of smooth bend plate diameter with sheathed specimens.	17

Figure 14. Strength loss as a function of rough bend plate diameter with sheathed specimens.	17
Figure 15. Smooth bend plate test results (strength vs. bend diameter) for sheathed and non-sheathed specimens.	18
Figure 16. Rough bend plate test results, strength vs. diameter, for sheathed and non-sheathed specimens.	18
Figure 17. A T-VIII static line with a single twist loaded in the bend test fixture.	21
Figure 18. Rupture strength as a function of the number of twists in a line.	22
Figure 19. Bar graph illustrating results extracted from Table 6.	23
Figure 20. Strengths of fatigue conditioned T-VIII and AbsorbEdge static lines compared to unused materials in both straight-pull and bend-plate configurations.	24
Figure 21. Precondition loading history, shown as load vs. displacement for a T-VIII web.	25
Figure 22. High-speed video frames of a T-VIII static line during rupture.	26
Figure 23. High-speed video of an AbsorbEdge static line during rupture.	27
Figure 24. Schematic of the T-VIII static line rolled and sewn webbing construction shown "seam side" up.	28
Figure 25. Schematic of the AbsorbEdge static line webbing construction, including longitudinally oriented tows of nylon shown in blue.	29
Figure 26. Failure region of the load-displacement curve for both materials using 0.500-in-diameter rough bend plate.	30
Figure 27. T-VIII specimen with 0.375-in-diameter rough bend plate. The absence of the transverse stitching is shown below the bend plate.	30
Figure 28. Load-displacement curves generated for T-VIII and AbsorbEdge specimens in the straight-pull configuration.	31
Figure 29. Failure region of the load-displacement curve for both materials using 0.500-in-diameter smooth bend plate.	32
Figure 30. Failure region of the load-displacement curve for both materials using 0.500-in-diameter rough bend plate.	32
Figure 31. Failure region of the load-displacement curve for both materials using 0.375-in-diameter smooth bend plate.	33
Figure 32. Failure region of the load-displacement curve for both materials using 0.370-in-diameter rough bend plate.	33
Figure 33. Failure region of the load-displacement curve for both materials using 0.250-in-diameter smooth bend plate.	34

Figure 34. Failure region of the load-displacement curve for both materials using 0.250-in-diameter rough bend plate.	34
Figure 35. Load-displacement traces of straight vs. rough 0.50-in bend pull for AbsorbEdge.	35
Figure 36. Load-displacement traces of straight vs. rough 0.50-in rough pull for T-VIII.	35
Figure 37. Unloaded specimens prepared with rows of perpendicularly oriented pins.	37
Figure 38. Bend fixture with a 0.500-in smooth bend plate, (a) T-VIII and (b) AbsorbEdge.	37
Figure 39. Bend fixture with a 0.500-in-diameter smooth bend plate loaded to ~2100 lb, (a) T-VIII and (b) AbsorbEdge.	38
Figure 40. Photographic record of the pin-test for T-VIII webbing (a) 20 s prior to failure, (b) 15 s prior to failure, and (c) 0.0010 s prior to failure.	39
Figure 41. Average specimen strength for various test conditions for both AbsorbEdge and T-VIII nylon webbing.	41
Figure A-1. Side view of straight and bend fixture gage lengths.	49
Figure A-2. Solid model of bend fixture and lower grip.	50
Figure A-3. Pin plate – aluminum.	51
Figure A-4. Plate holder – steel.	52
Figure A-5. Side rail – aluminum.	53
Figure A-6. Top plate – aluminum.	54
Figure A-7. Trolley anchor – steel.	55
Figure A-8. Trolley side plate (left) – aluminum.	56
Figure A-9. Trolley side plate (right) – aluminum.	57
Figure A-10. Trolley stop – aluminum.	58
Figure A-11. Trolley rail – aluminum.	59
Figure A-12. Typical bend plate – steel.	60
Figure B-1. Load vs. displacement curves for test set 1 of T-VIII webbing.	61

INTENTIONALLY LEFT BLANK.

List of Tables

Table 1. Properties for nylon static line material determined by DSC investigation.	8
Table 2. Tensile test rupture results for straight, bent, and cotton-sheathed lines.....	13
Table 3. Bend test results using Kevlar, nylon, and Teflon sheaths.....	19
Table 4. Performance of various sheathing materials compared to the standard cotton sheaths.	20
Table 5. Test results for twisted static lines.	21
Table 6. Results of wet static line bend tests.....	22
Table 7. Test results for preconditioned static line material.....	24
Table 8. Percent improvement of AbsorbEdge as compared to T-VIII for various tests conditions.....	40
Table A-1. Table of minimum gage lengths.....	49
Table B-1. Statistics report for test set no. 1, T-VIII webbing.	61

INTENTIONALLY LEFT BLANK.

1. Introduction

In U.S. Army personnel airdrop operations, a static line assembly, as shown in Figure 1, is used to connect the anchor line cable inside the jump aircraft to the parachute and pack worn by the jumper. When parachute riggers pack the parachute, they attach the apex of the canopy to one end of the static line with 1/4-in cotton tape, pack the canopy in a deployment bag, and close the deployment bag within the flaps of the pack tray by tying a length of 1/4-in cotton tape through the flap closing loops and the pack opening loop on the static line. The static line is then stowed outside the pack flaps. As jumpers prepare to exit an aircraft, they partially unstow the opposite end of the static line and attach the snap hook at that end of the static line assembly to the anchor line cable inside the jump aircraft. When jumpers exit, the remainder of the static line is unstowed as the jumpers fall away from the aircraft. When the line is extended to the pack opening loop, it transmits a force (typically not exceeding 400 lb) sufficient to sever the pack closing tie. The static line then extends to its full length and withdraws the deployment bag from the pack tray. The suspension lines of the canopy then deploy from their stows on the deployment bag, the canopy is drawn out of the deployment bag until line stretch is achieved, and the tie connecting the end of the static line to the apex of the canopy is severed. This typical pattern of parachute deployment can be interrupted if the jumper or his equipment becomes entangled with the static line as it is unstowed. In such cases, various factors (jumper weight, location of entanglement, etc.) may interact and result in the rupture of the static line requiring the jumper to deploy his or her reserve parachute in order to prevent a fatal high-velocity impact with the ground. In other cases, the static line may absorb the energy generated as a result of the entanglement and retain, or "tow," the jumper outside the aircraft. Personnel onboard the aircraft must then activate emergency procedures to retrieve the towed jumper inside the aircraft.

The static line that has been used by U.S. military forces during the last several decades is constructed from 1 23/32 PIA-W-4088A [1] Type VIII (T-VIII) nylon webbing rolled and sewn to a width of ~3/4 in and a length of ~15 ft. Figure 2 depicts an onboard view of a T-VIII static line extended with some tension in the line. The static line begins at the anchor line cable and bears against the door edge as it passes to the outside while the jumper exits and falls below and to the rear of the aircraft. In this configuration, the line strains longitudinally (elongates) and translates transversely while in contact with the edge of the aircraft door. The line will form an angle of 90° or more as it passes around the aircraft door and may be subject to various imperfections along the surface of the

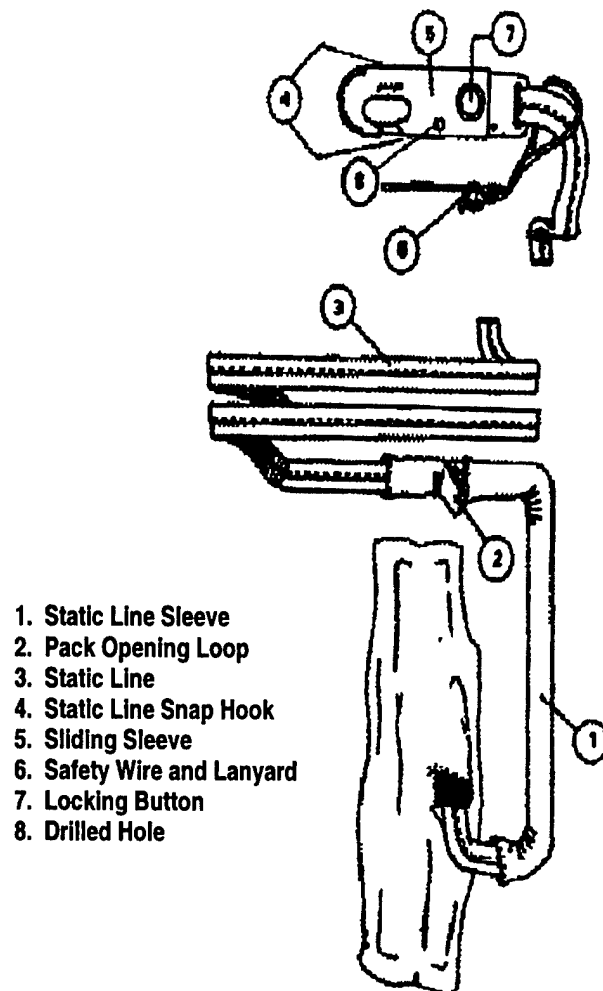


Figure 1. Basic components of the T-VIII static line system [2].

door edge (despite a prejump inspection of the surface and application of tape to minimize imperfections). Many static lines that have ruptured as a result of jumper entanglement with the line have broken at the point where they were in contact with the door edge.

Remnants of two such ruptured static lines were analyzed as part of this investigation to determine whether their material properties had been degraded as a result of previous usage. Results of these analyses indicated that the cause of both failures was most likely due to mechanical overload of the line rather than any degradation of their material properties.

As a result of these findings, a series of experimental tests was performed to determine the sensitivity of the T-VIII static lines to simulated airdrop operating conditions. The objectives were to identify and determine the effect of static line strength reducing conditions encountered in airdrop operations.

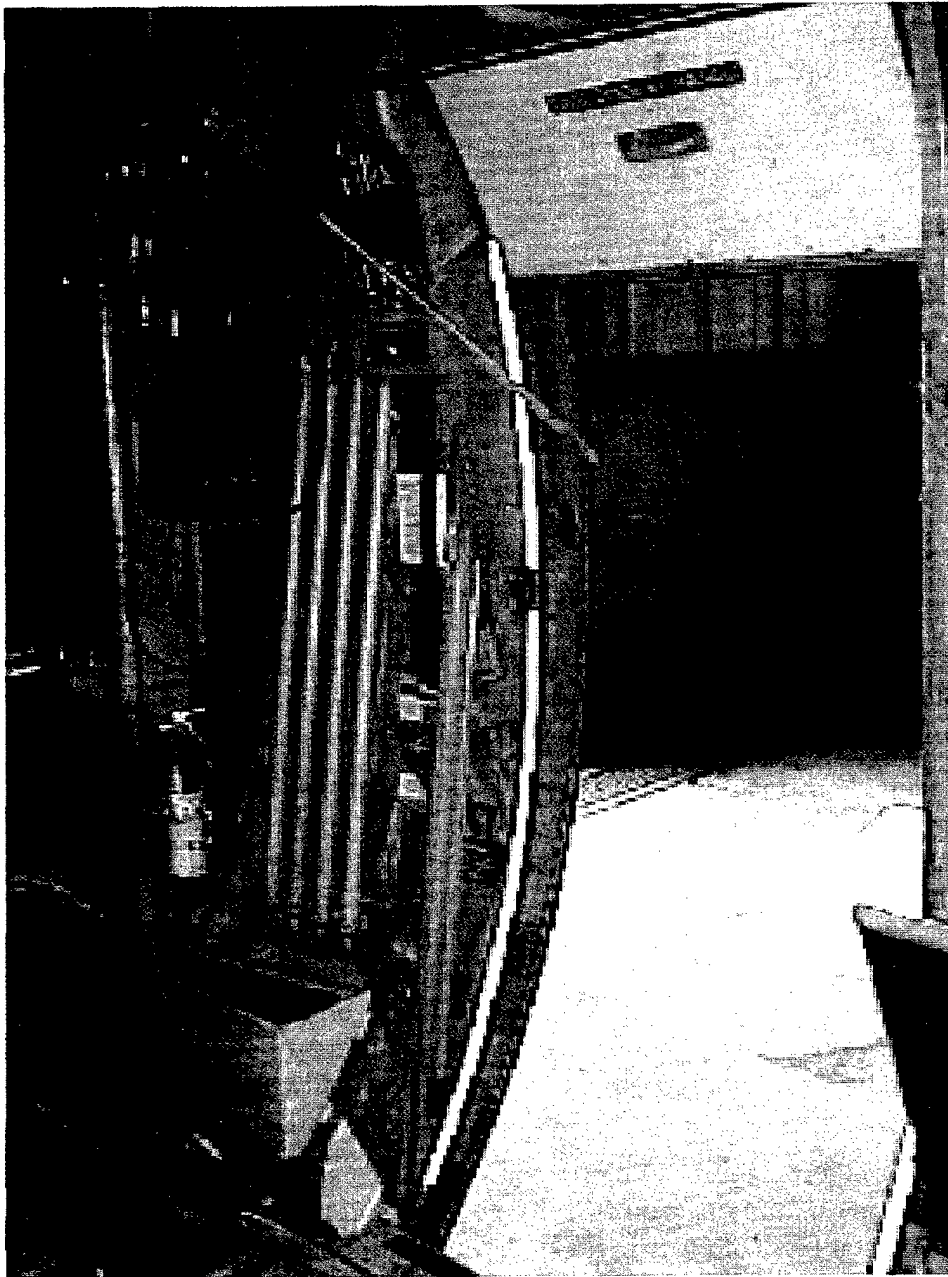


Figure 2. Onboard view of a static line extending out of an aircraft door in the postjump, preparachute deployment configuration.

Additionally, the performance improvement of sheathing static line material was to be investigated in an effort to demonstrate its benefits and applicability to fielded systems.

Straight-pull tensile tests were performed to establish the average baseline rupture strength of the T-VIII webbing material. Straight-pull tests were performed subject to minor variations of guidelines established in Federal Test

Standard 191A (Method 4108) [3]. A test fixture, designed to load the webbing material in tension around a 90° bend, was fabricated and used to simulate the interaction between the static line and the edge of an aircraft door. Plates of various thicknesses featuring both smooth and knurled semi-cylindrical bearing surfaces were used in the fixture to determine specimen sensitivity to bend radius and to contact surface texture (friction). Other variables were investigated, including the number of twists in a line, retained water in a line, mechanical fatigue, and the performance improvements from sheathing materials including cotton, Kevlar, nylon, and Teflon. Strength reductions due to the variables previously identified were contrasted against the baseline strength.

A proposed replacement for the T-VIII webbing material, referred to as AbsorbEdge,* was tested and evaluated in accordance with an identical test matrix.

2. Characterization of Failed Static Line Material

Remnants of two static lines that had ruptured during personnel parachute jumps were examined to determine if material property degradation had contributed to the static line failures. Differential scanning calorimetry (DSC) testing techniques were applied to the ruptured line remnants as well as to a quantity of unused material obtained directly from the manufacturer.

Fiber samples were taken from the "failure zone" and from the "bulk matrix zone" of each failed line. Failure zone specimens feature fractured, frayed, and plastically elongated fibers. Bulk matrix zone samples are undamaged fibers cut from the nylon specimen. In all samples, bulk matrix fibers were obtained at a minimum distance of 2 in from a failure zone. A bulk matrix specimen was extracted from each of the ruptured static line remnants in order to determine the environmental exposure damage of the used nylon for comparison with original factory material. Original factory material was tested in both the naturally processed white color and in the end-item yellow-dyed color.

DSC evaluations were performed on a TA Instruments 2980 DSC using a temperature ramp of 10 °C/min and a cool-down rate of 20 °C/min. Experimental runs were performed for each of the samples to identify both the glass transition (T_g) and the crystalline melt (T_m) temperatures. For commercially available nylons, these temperatures are well known and characteristic of material composition and processing history. The DSC evaluations allowed easy determination of the nylon thermal parameters. Deviation from standard thermal signature, e.g., a shift in T_g or T_m , can result from polymer reorientation,

* AbsorbEdge is a registered trademark of Elizabeth Webbing Mills Co., Inc., Central Falls, RI.

degradation, or compositional change resulting from processing or environmental exposure. Moisture absorption, exposure to excessive ultraviolet (UV) radiation or ozone, thermal cycling, chemical contamination, and mechanical (plastic) drawing are typical causes of changes in the thermal signature and are detectable by noting DSC shifts in position or intensity of the T_g or T_m . In some instances, stimuli and/or causes such as those previously identified relate directly to the strength and ductility (toughness) of nylon currently used in the static line systems.

DSC results of failure zone samples taken from the ruptured lines are shown in Figure 3. Plots of heat flow vs. temperature feature the characteristic change in heat flow (depression and recovery) associated with the melting of polymer crystals (T_m) between 210° and 270 °C. The T_g onset of both specimens is ~50 °C (T_g [nylon 6] = 47 °C, T_g [nylon 6,6] = 50 °C) using a 10 °C/min ramp rate. Comparing both T_g and T_m with handbook values allows conclusive determination that the low T_m line is nylon 6 (poly ϵ -caprolactam), and the other line is nylon 6,6 (poly[hexamethylene adipamide]). These polymer assignments were further confirmed by noting the presence of color-coded tracers stitched into the ruptured cords. For these lines, it was determined that the manufacturer used a black stringer to designate the nylon 6,6 material and a red stringer to denote a nylon 6-based line system. One of each had failed and been examined with experimental results in complete agreement with the manufacturer's color-coding system.

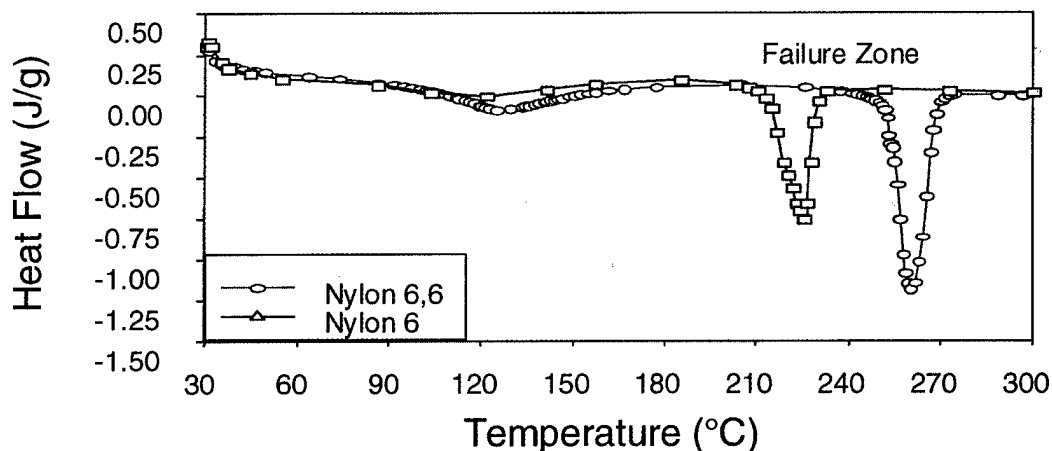


Figure 3. DSC investigation of two field failed nylon jump cords demonstrating the effective use of thermal characterization for discerning compositional differences in the two materials. Assignment of each of the polymer fibers is shown in the legend.

DSC results of bulk (cut zone) and failure zone samples taken from the nylon 6 line are shown in Figure 4 with a reduced temperature range for the crystalline melting transition T_m shown in Figure 5. Comparing the experimental result shows that no significant differences are present between either the melting or glass transition temperatures of the two samples. The slight variations in melting temperature indicate that a small variation in the crystallite content or crystal domain size is possible. However, these small inconsistencies are not significant (3–5%) and are typically the result of accumulated errors from the sample size, sampling technique, and instrumental error. For instance, sheared surfaces generated during sample extraction with scissors, selection of fibers for sampling, and packing of fibers in the sample pan all contribute to thermal transfer differences between the polymers and the instrument which can result in as much as 5% sample variation. The variations observed in Figures 4 and 5 are common among samples from a same-source with known loading histories.

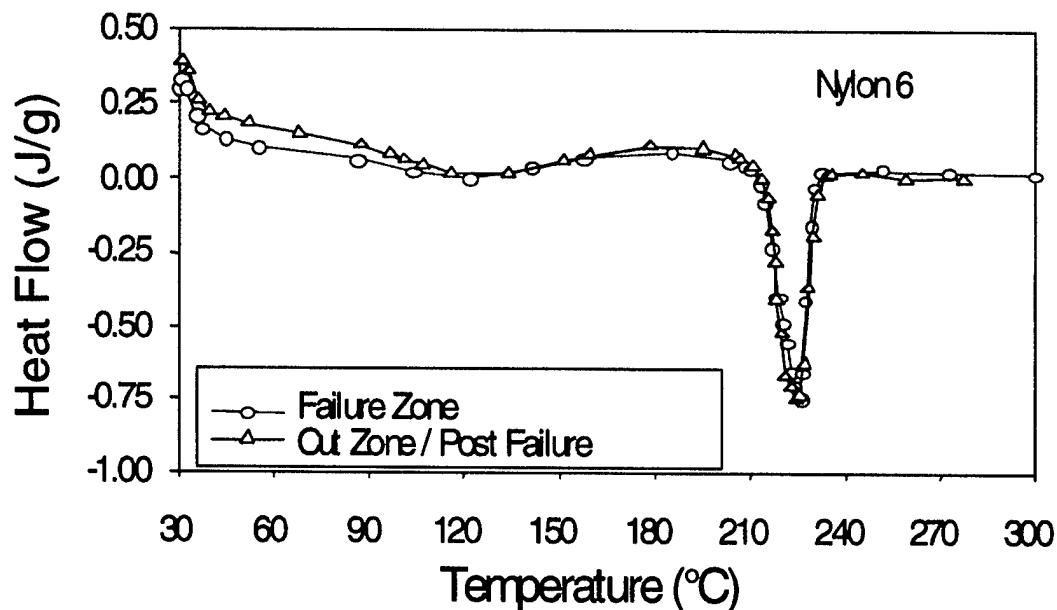


Figure 4. DSC trace of nylon 6 from room temperature through the crystalline melting point of nylon ropes. Agreement between results measured in and far from the failure zone for a single rope is excellent.

Results of the DSC test performed on the nylon 6,6 line are shown in Figure 6. This figure reports results of failure and bulk zone samples, as well as results obtained from unused factory specimens. The unused samples were determined to be nylon 6,6 via independent DSC testing and are included to demonstrate the insignificant differences between the signature characteristics (DSC plots) of the unused vs. used material samples. Figure 7 is an enlargement of the T_m zone of for nylon 6,6 sample. Note that the DSC analysis did detect a slight difference

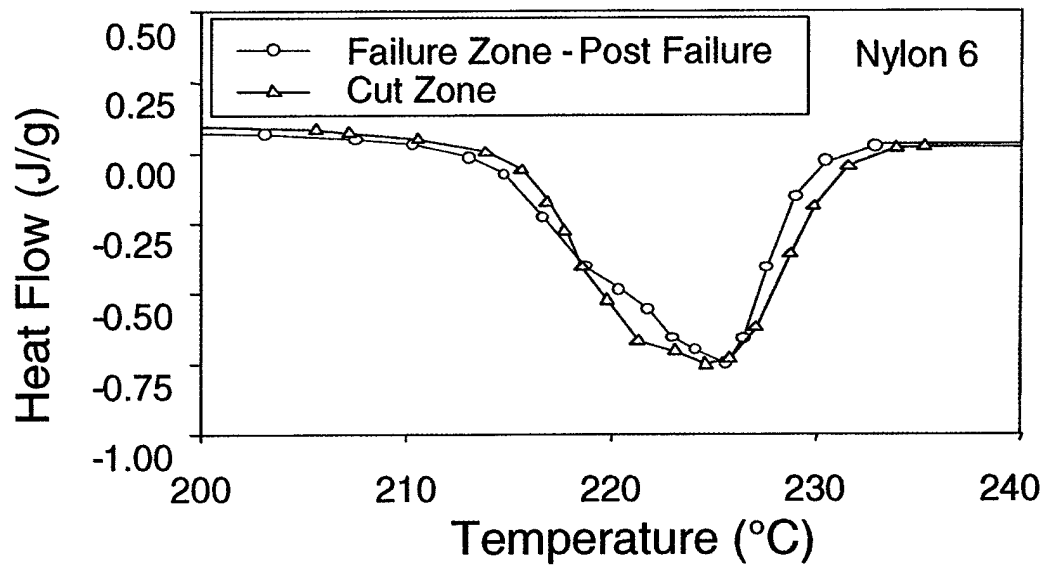


Figure 5. Crystalline melting traces of fielded nylon 6 jump cords determined using DSC. Fielded samples show no substantive variations between bulk matrix fibers attained far from the failure zone and fibers extracted from the failure zone.

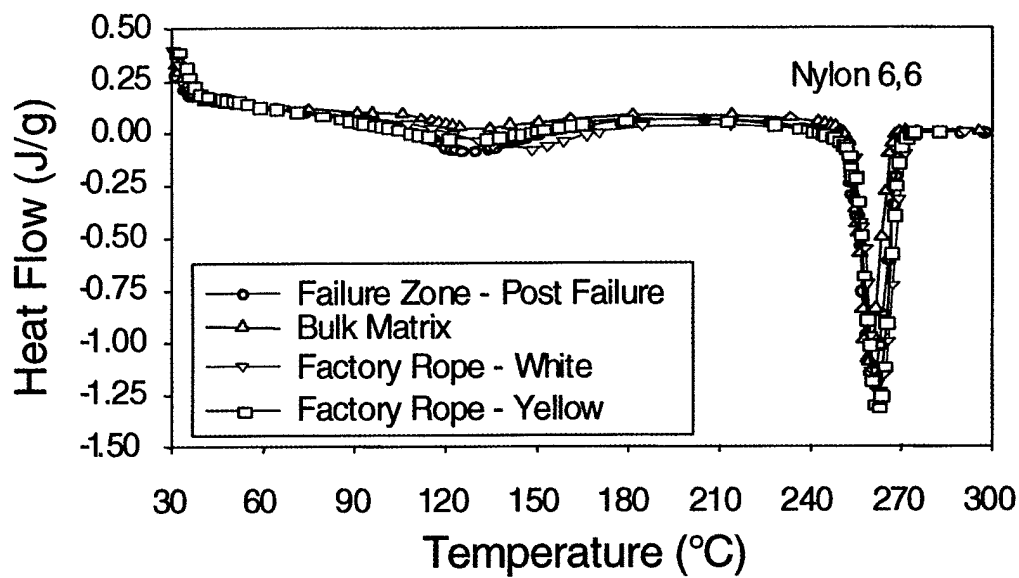


Figure 6. DSC trace of nylon 6,6 from room temperature through the crystalline melting point of nylon ropes. Agreement between various samples is excellent.

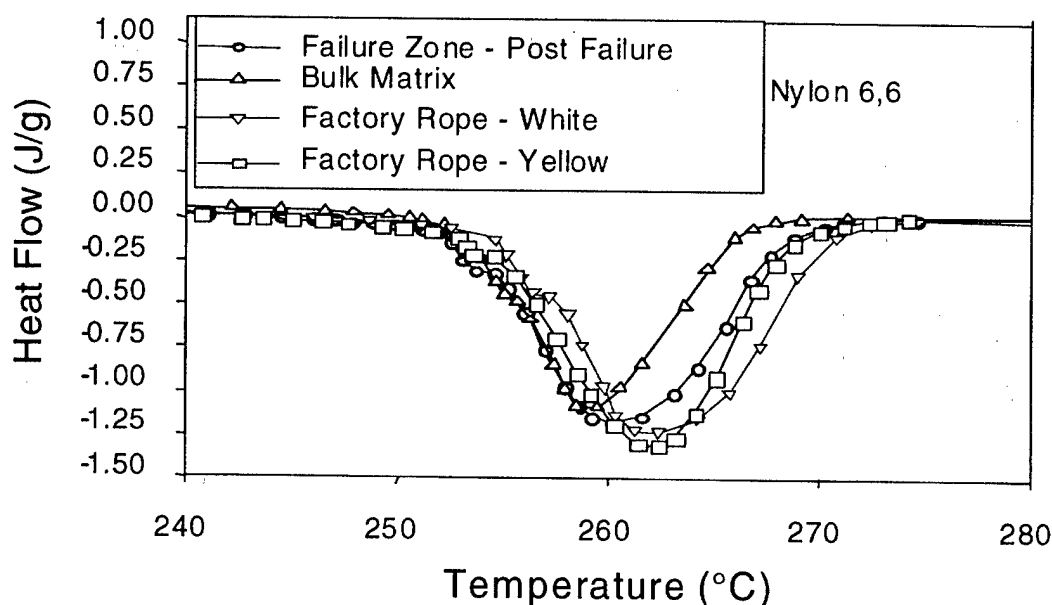


Figure 7. Crystalline melting region for nylon 6,6-based jump cords showing minimal deviations in crystalline structures for factory original vs. field failed cords.

between the white vs. unused yellow nylons. This difference, potentially arising from the coloring process or additives, is again comparable to the difference between bulk and failed fiber samples and is still within the experimental error margin of the measurements. Given that the fielded static lines are colored, any variations between the fielded lines and the non-dyed factory sample (Factory Rope—White) were disregarded. A summary of DSC test result data for both nylon types is shown in Table 1.

Table 1. Properties for nylon static line material determined by DSC investigation.

Nylon Type	Condition	ΔH_m (J/g)	T_m (peak) (°C)	T_m (onset) (°C)
6,6	Bulk Matrix	77.7	259.0	254.2
	Failure Zone	81.4	260.3	253.9
	Factory—White	82.5	261.8	256.5
	Factory—Yellow	79.9	262.0	254.1
6	Failure Zone	50.6	225.5	213.5
	Cut Zone	54.0	224.7	215.5

3. Assessment of DSC Results

DSC analysis results indicate that both failed lines ruptured for reasons other than those related to material property degradation. No apparent (DSC detectable) change in the base material properties occurred as a consequence of field use. It would appear, therefore, that the static line failures either occurred as a result of mechanical overload or due to progressive and excessive tearing. This assumes that the unused factory material, used as a standard to contrast the quality of the used lines, is suitable in terms of strength and ductility for static line applications and functions as a reasonable baseline comparison. Results of thermal investigations of factory materials indicate that this should be a valid assumption.

The geometric configuration assumed during entanglements occurring from side door exits of fixed-wing aircraft would include a right ($\sim 90^\circ$) angled bend around the edge of the aircraft door. In this configuration, the line must sustain the high tensile force applied by the jumper's weight (in a turbulent/random air stream) combined with localized abrasion from contact with the door edge. Initial high-magnitude shock waves could propagate from the terminals of the line and possibly superimpose at the door edge where reaction forces are applied. Tearing could initiate when the resulting transverse load (door edge) abrades or damages groups of load-bearing fibers. Progressive damage would result to adjacent fibers as the tensile load is redistributed to surviving fibers. The progression of damage would continue until the quantity of surviving fibers is not sufficient to sustain the tensile load resulting in catastrophic failure.

4. Tensile Testing of Static Line Webbing Material

Conventional straight-pull tensile tests were initially conducted in accordance with Federal Test Standard Number 191A (Method 4108) [3]. The test method details the specifics of the specimen grips and requires a crosshead displacement (or strain rate) of 3.0 ± 1.0 in/min.

In particular, the method requires that 4-in-diameter split drum grips be employed during testing. The split drum grips consist of a pair of longitudinally split semi-cylinders. One semi-cylinder is rigidly mounted to the test fixture yoke, while the other is allowed an eccentric rotational degree of freedom. Common to each semi-cylinder is a flat surface that mates with the flat surface of the opposing semi-cylinder. The specimen is wrapped (in a helical fashion)

around the curved outer surface of the mating semi-cylinder with the excess material positioned between the flat clamping (self-locking) surfaces.

Straining of the specimen is both maximum and uniform between the grips and progressively fades to zero along the surface of the cylinders. With an anticipated specimen elongation (to failure) of 20–30%, the required crosshead displacement of the test machine was estimated to approach 10.5 in. Compliance with this configuration requires specimens of ~48-in lengths (including the two lengths of specimen wrapped helically around each grip plus the 8.6-in gage length between grips). Preliminary testing proved that these estimates were correct. Appendix A offers detailed drawings showing gage lengths and grip components.

5. 90° Bend Testing Procedure

Tensile tests were performed using a 90° bend fixture to determine the adverse effect of loading static lines in tension around a 90° bend while bearing against a specified contact edge radius. This test configuration functioned as a limited simulation of a static line in contact with the door edge of an aircraft. Transverse bend loads were applied to the static line specimens by contact with bearing plates mounted in the test fixture. Two sets of plates, featuring both smooth and diamond-knurled semi-cylindrical bearing surfaces, were used in the fixture. The bearing surfaces for both sets include bend diameters of 0.250, 0.375, and 0.500 in. Knurling steel rod stock and welding the rod onto the end of a similar thickness plate completed the fabrication of the rough surface plates. The plates were mounted in the fixture such that the curved bearing surfaces extended away from its support fixture at a 45° angle. This configuration prevented static line contact with any other part of the fixture during testing, as can be seen in Figure 8. A complete set of component drawings along with the assembly drawing is shown in Appendix A.

For bend fixture testing with the 4-in grips, the total specimen gage length accumulates to ~61 in, which consists of a 13.5-in span between the bend plate and the upper grip with a 10-in span between the bend plate and the lower grip and the helical wraps around both upper and lower grips (Figure 9[a]). Straining to failure with a gauge length of 61 in could not be achieved with both of the existing 4-in-diameter grips and crosshead displacement limits of the test frame. Consequently, a pair of 2-in-diameter grips were fabricated and installed in the fixture to reduce the active gage length to about 48 in and, hence, the approximate accumulated elongation to rupture to 10 in (achievable in the test frame).

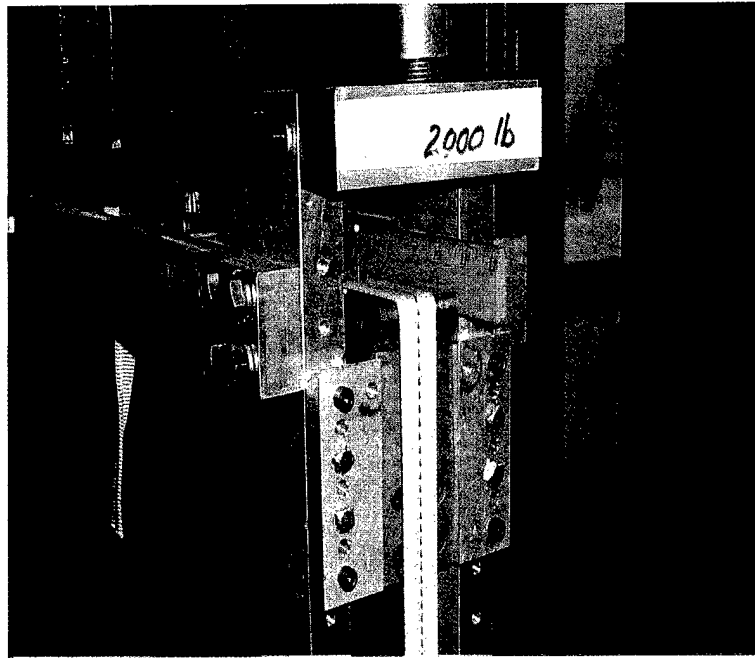


Figure 8. The 90° bend fixture loaded with a static line specimen at ~2000 lb.

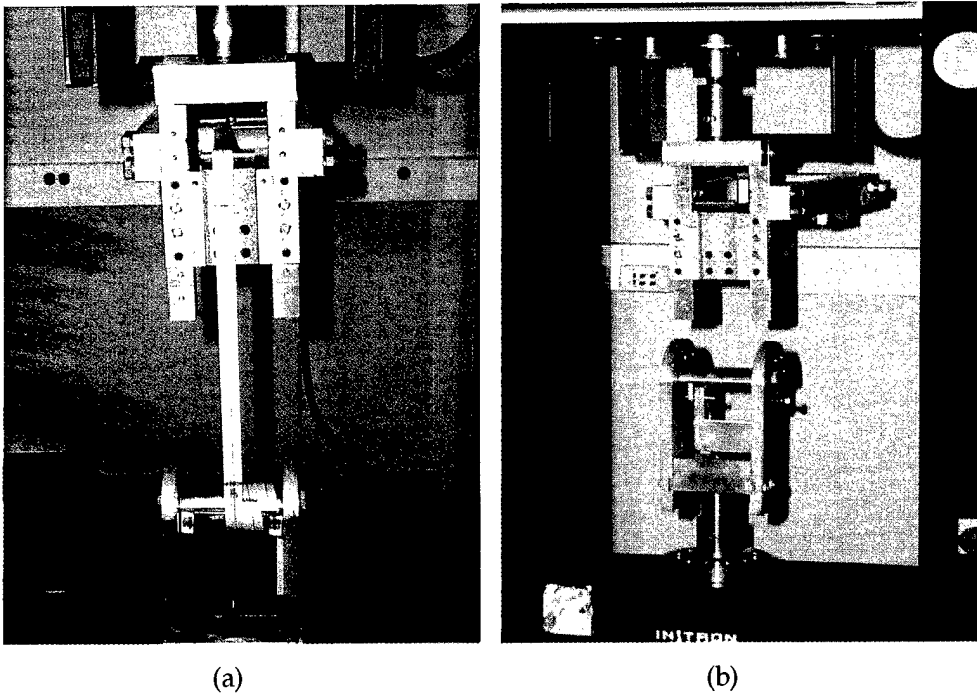


Figure 9. The 90° bend fixture (a) loaded with a static line (note the green pen marks on the specimen indicating the original position of contact with the bend plate and the position of the lines relative to the split in the grip) and (b) unloaded with the lower grip in the open position.

Practice tests validated that the straight-pull test results were not sensitive to the smaller 2-in-diameter grips. In an attempt to reduce the number of test variables between the two test configurations (straight and bent), the 2-in grips were adapted as a standard for all testing.

Specimens tested in the bend fixture were loosely wrapped around the lower grip with a double helical wrap. The end of the specimen was placed between the flats of the grip and pulled tight by the test operator. An additional 6-in section of specimen was placed in the flats of the grip opposite the side that clamps the specimen. This procedure was a routine practice adopted to ensure that the mating semi-cylinders maintained parallel flat clamping surfaces. The remainder of the specimen was then placed over the bend plate and pulled tightly to the upper grip. At the upper grip, a single helical wrap around the grip surface was made prior to inserting the end into the flats. A sufficient length of excess material was included with each specimen so the test operator could grasp and manually apply a tensile load while a second operator positioned the test-frame crosshead to the "zero" position (a downward displacement of ~1.5 in). This practice applied a preload of ~60 lb for T-VIII material and ~120 lb for the AbsorbEdge. Marker lines were then drawn on the specimens at locations where the specimens crossed and entered the flats of both grips as well as at the location where contact was made with the bend plate. Test operators visually monitored the pen marks to assure that slipping (at the opening to the grip flats) did not occur in either grip during testing.

Figure 8 depicts an AbsorbEdge specimen loaded to ~2000 lb with the 0.375-in smooth plate mounted in the bend fixture. Figure 9(a) and (b) show the front view of the fixture loaded and unloaded, respectively.

The first series of bend tests performed with this fixture were intended to determine the sensitivity of both static line material systems to the various bend diameters (0.500, 0.375, and 0.250 in). Both smooth and knurled bend plate surfaces were used in the evaluation. Cotton sheathing material was applied to both materials to test for any beneficial effect they may have in conserving straight-pull strength by reducing friction and/or by increasing the bend radius.

6. Tensile Test Results

6.1 Performance of T-VIII and AbsorbEdge Webbing in Straight, Bent, and Cotton-Sheathed Test Configurations

Table 2 reports the rupture strength test results for the straight-pull and bend-pull tests. Straight-pull test results are reported at the top of the table (test sets 1 and 2) and are used as a value against which results for all other test configurations are compared. An actual load vs. elongation test series result (test set 1) is presented in Appendix B.

Table 2. Tensile test rupture results for straight, bent, and cotton-sheathed lines.

Straight- and Bend-Pull Static Line Rupture Strengths										
A	B	C	D	E	F	G	H	I	J	
Test Set	No. Tests (count)	Material	Bend Diameter (in)	Surface	Sheathing	Rupture Load (lb)	Standard Deviation (lb)	Elongation (in)	Result/Straight (ratio)	
1	5	T-VIII		Straight-Pull Test		4439	262	9.954	NA	
2	5	AE		Straight-Pull Test		5667	145	6.511	NA	
3	5	T-VIII	0.500	Smooth	None	4285	85	10.179	0.97	
4	5	AE	0.500	Smooth	None	5089	24	9.09	0.90	
5	5	T-VIII	0.500	Smooth	Cotton	4082	111	12.09	0.92	
6	5	AE	0.500	Smooth	Cotton	5024	64	10.462	0.89	
7	5	T-VIII	0.500	Knurled	None	1989	95	7.669	0.45	
8	5	AE	0.500	Knurled	None	2846	148	6.888	0.50	
9	5	T-VIII	0.500	Knurled	Cotton	4324	82	10.536	0.97	
10	5	AE	0.500	Knurled	Cotton	5065	100	9.026	0.89	
11	5	T-VIII	0.375	Smooth	None	2682	113	9.349	0.60	
12	5	AE	0.375	Smooth	None	3985	63	8.946	0.70	
13	5	T-VIII	0.375	Smooth	Cotton	4073	78	11.388	0.92	
14	5	AE	0.375	Smooth	Cotton	4795	66	9.858	0.85	
15	5	T-VIII	0.375	Knurled	None	2323	80	9.245	0.52	
16	5	AE	0.375	Knurled	None	3167	77	8.122	0.56	
17	5	T-VIII	0.375	Knurled	Cotton	4120	72	12.136	0.93	
18	5	AE	0.375	Knurled	Cotton	4996	44	10.452	0.88	
19	5	T-VIII	0.250	Smooth	None	2410	45	8.207	0.54	
20	5	AE	0.250	Smooth	None	3772	69	7.224	0.67	
21	5	T-VIII	0.250	Smooth	Cotton	3147	313	9.328	0.71	
22	5	AE	0.250	Smooth	Cotton	4448	161	10.199	0.78	
23	5	T-VIII	0.250	Knurled	None	2276	33	9.064	0.51	
24	5	AE	0.250	Knurled	None	3201	83	8.077	0.56	
25	5	T-VIII	0.250	Knurled	Cotton	3997	75	11.626	0.90	
26	5	AE	0.250	Knurled	Cotton	4725	66	10.062	0.83	

Notes: T-VIII = Type VIII.
 AE = AbsorbEdge.
 NA = Not applicable.

The force reported in rupture load column G of Table 2 is the load required to rupture the line in the specified test configuration. Each rupture load entry, unless otherwise noted, is the statistical mean of five consecutive tests. This sampling size (column B) is stipulated in Federal Standard 191-A [3].

Table 2, column J, reports the ratio of the bend test results of column G to the straight-pull test results (test set 1 for T-VIII and test set 2 for AbsorbEdge). The bend- to straight-pull ratio reported in column J is an indicator of the fraction of original straight-pull strength retained for the specified load condition. An ideal strength retention ratio would be unity.

The rupture strengths from Table 2 are shown schematically in Figure 10. The axis designators "S" and "R" refer to smooth and rough textured (knurled) plates, respectively. The "90" refers to the test configuration, specifically, the 90° bend fixture. It is apparent from these results that the static line strengths are reduced as a consequence of the 90° bend angle. Further, for smooth bend plates, the strengths of both sheathed and unsheathed lines are reduced as the bend diameter is decreased. For the rough textured bend plate tests, however, the results are mixed. Sheathed static lines had a similar sensitivity to bend diameter (barring the marginal outlier of test sets 15 vs. 23). However, with a reversal in this trend, unsheathed static lines had the lowest strength with the larger diameter rough contact surface.

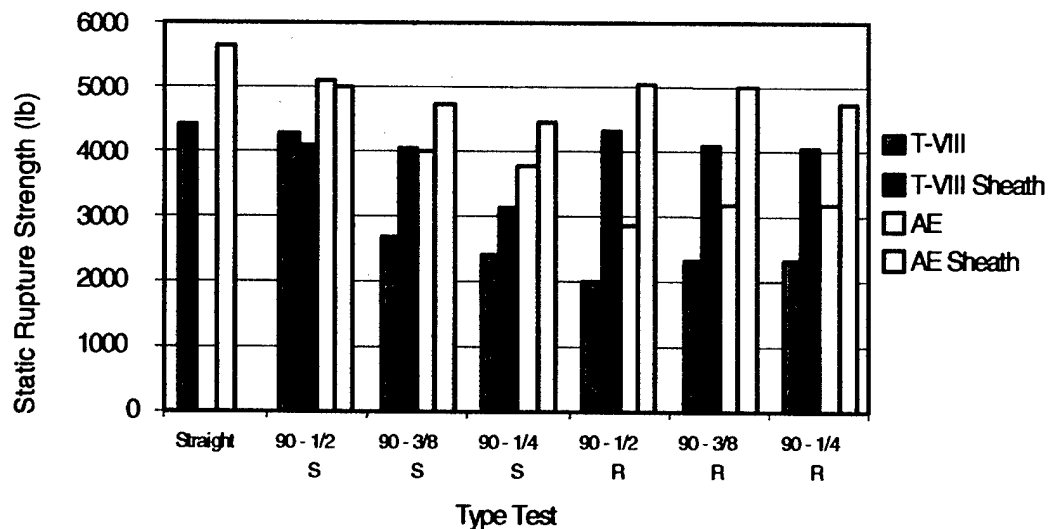


Figure 10. Test results extracted from Table 2 showing trends of strength as a function of bend plate diameter and texture both with and without cotton sheathing.

Based on experimental results, cotton sheathing applied to both the T-VIII and AbsorbEdge materials reduced the severity of the strength loss as compared to non-sheathed specimens.*

The trend for decreasing strength with decreasing bend diameter held for all sheathed static line test configurations. It is also true that in all non-sheathed test cases, the smooth bend test specimens reported higher rupture strengths than the rough bend specimen for each of the three bend diameters. Finally, it is observed that the AbsorbEdge material reported higher rupture strengths than the T-VIII material for any given set of test parameters. This is consistent with the straight-pull results reported for test sets 1 and 2.

Figure 11 summarizes the trend of strength loss as a function of bend plate diameter for the non-sheathed T-VIII and AbsorbEdge materials. The rupture strengths from bending are compared to straight-pull strength results.

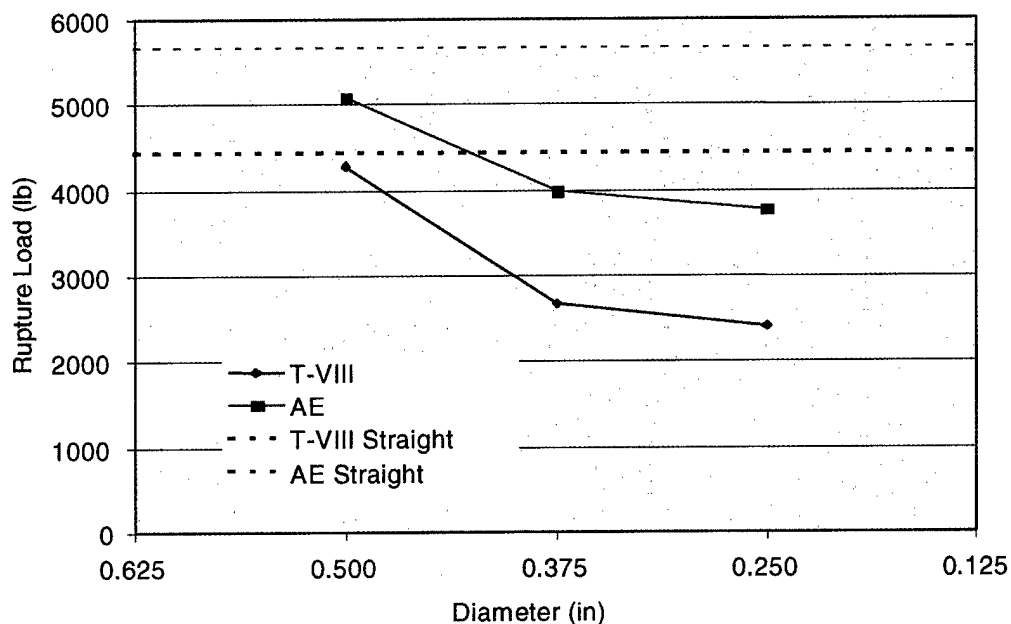


Figure 11. Strength reduction as a function of smooth bend plate diameter.

Figure 11 demonstrates a severe reduction in the strength for both materials between the 0.500- and 0.375-in-diameter bend plates (steep slope). Between the 0.375- and 0.250-in-diameter plates, however, the reduction in strength is not as severe (5–10%). Observe that the T-VIII material exhibits a more dramatic reduction in strength than the AbsorbEdge as bend diameter decreases.

* Note that test sets 3 and 5 from Table 2 are an exception to this trend.

Figure 12 is a plot of non-sheathed static line specimen strength tested with rough textured bend plates. A significant reduction in strength is observed in both types of lines over the rough 0.500-in-diameter surface. The trend of increased strength loss as a function of decreasing bend diameter (the case with smooth bend plates) has been reversed for the rough surface condition. This may be due to the increase in abrasive contact area (destructive area) between the static line and large diameter bend plates and a smaller destructive area associated with smaller diameter bend plates.

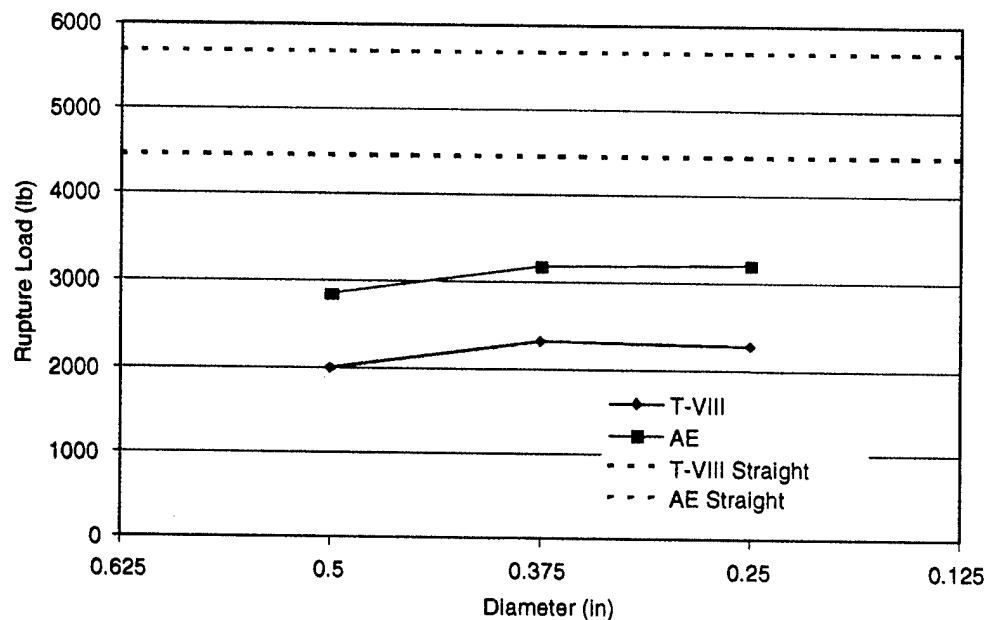


Figure 12. Strength of static lines tested with rough bend plate diameter.

In the case of sheathed specimens tested over smooth bend plates, a linear relationship is valid for the AbsorbEdge but not valid for the T-VIII. The T-VIII line with a cotton sheath behaves in a much less consistent manner. It should be noted, however, that the addition of cotton sheathes raised the rupture strength of each material tested in the bend configurations from their lower non-sheathed rupture strengths. This is true for all cases except for the T-VIII case with 0.500-in-diameter smooth surface (a possible outlier based on statistical results). Figure 13 illustrates the strength loss for bend tests conducted with smooth plates and sheathed lines.

The improvement in strength for specimens protected with cotton sheathes and tested over rough textured bend plates is quite apparent and more consistent than those tested over smooth plates without sheaths. A noticeable improvement in strength is observed for both materials and the trend of sensitivity to bend diameter is maintained. Figure 14 illustrates the results for rough bend plates and cotton-sheathed specimens.

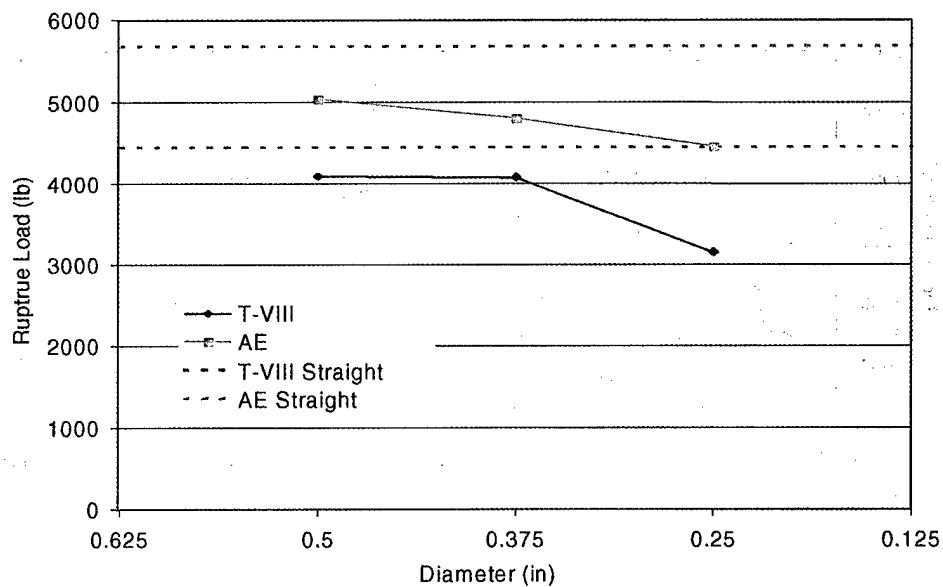


Figure 13. Strength loss as a function of smooth bend plate diameter with sheathed specimens.

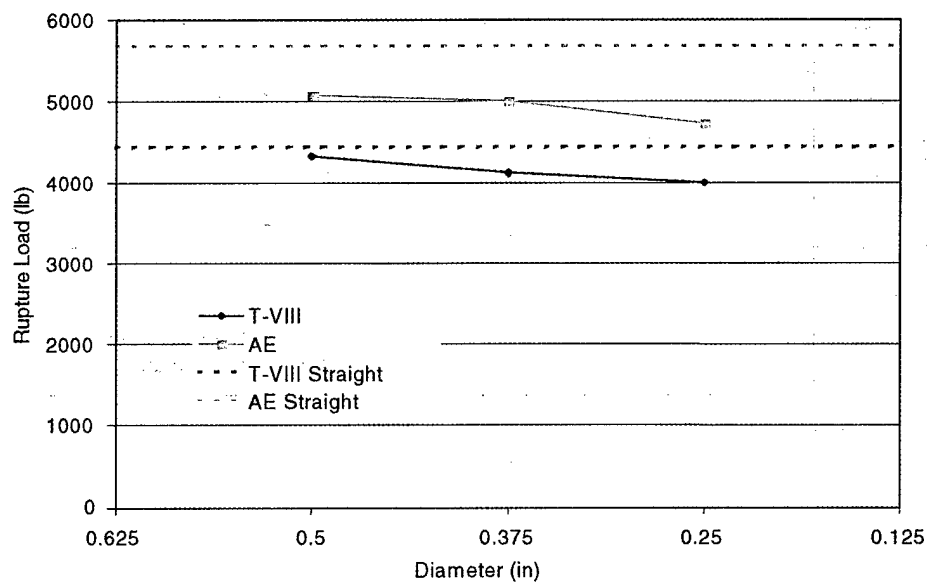


Figure 14. Strength loss as a function of rough bend plate diameter with sheathed specimens.

To demonstrate the effect of sheathing, Figures 15 and 16 show the strengths of the sheathed and unsheathed static lines as a function of the bend diameter for smooth and rough bend plates, respectively. Notice that in Figure 15, the addition of sheathing not only raised the rupture strength for each material but also reduced, somewhat, the nonlinear behavior of the T-VIII line. Additionally,

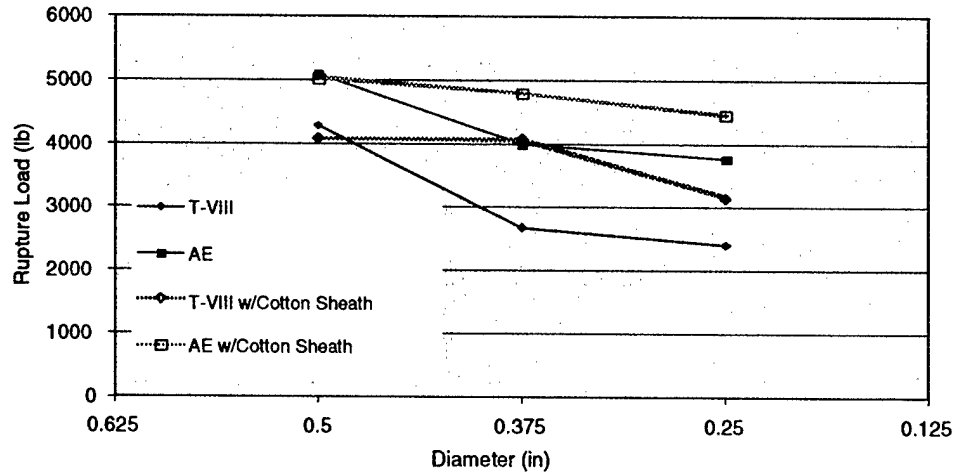


Figure 15. Smooth bend plate test results (strength vs. bend diameter) for sheathed and non-sheathed specimens.

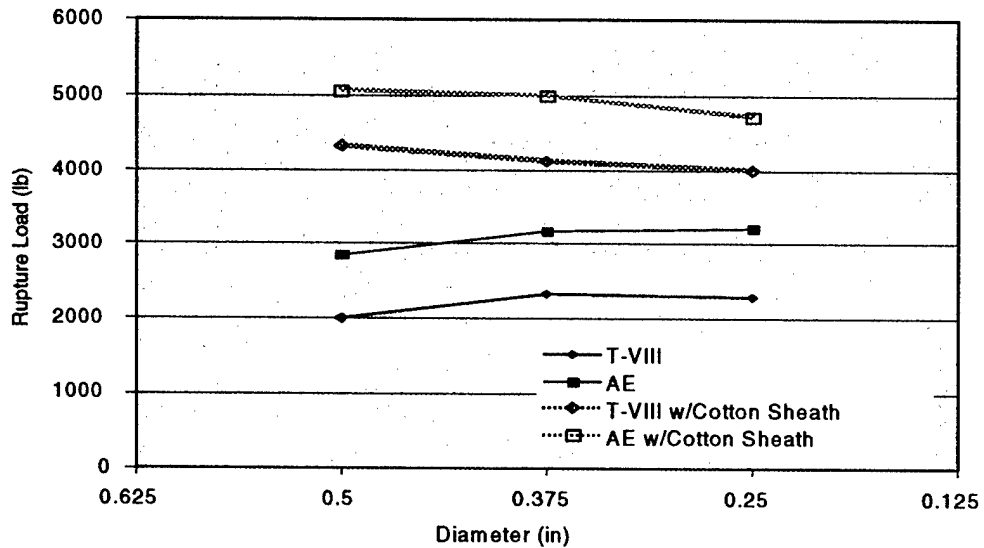


Figure 16. Rough bend plate test results, strength vs. diameter, for sheathed and non-sheathed specimens.

the slopes of the trends (strength vs. diameter) have a negative concave up slope for non-sheathed specimens and a negative concave down slope for the sheathed specimens. In effect, this implies that the sensitivity of the specimens to a change in bend diameter has been altered over the range of diameters by the addition of the cotton sheaths (non-sheathed—sensitive to larger diameters; sheathed—sensitive to lower diameters).

Figure 16 demonstrates the effect of sheathing over rough surfaces. In this figure, results were plotted for both materials in the sheathed and non-sheathed configurations tested with the rough bend plates. The sheathing increased the rupture strength of each material tested in the bend configuration significantly. The inconsistent trend of increasing strength with decreasing bend diameter, observed for the unsheathed lines on rough surfaces, is reversed when sheaths were implemented. Again, AbsorbEdge reported higher rupture strengths than the T-VIII material in all cases.

6.2 Teflon, Nylon, and Kevlar Sheath Tests

Polymer-based sheathing materials were tested with both static line materials in the bend fixture. A limited quantity of Kevlar, Teflon, and nylon sheathing material, acquired from the Bally Ribbon Mills, was used with the 0.500-in- and 0.375-in-diameter smooth bend plates. Results of these tests are reported in Table 3. Note that due to material supply limitations, only two or three samples, rather than the preferred five samples, per set were used for some experimental configurations (see column B).

Table 3. Bend test results using Kevlar, nylon, and Teflon sheaths.

Polymer-Based Sheath Test Results								
A	B	C	D	E	F	G	H	I
Test Set	Specimens (count)	Material	Plate Dia. (in)	Surface	Sheathing	Rupture Load (lb)	Std Dev. (lb)	Elongation (in)
27	5	T-VIII	0.5	Smooth	Kevlar	4331	203.24	11.99
28	5	AE	0.5	Smooth	Kevlar	5005	129.14	10.23
29	5	T-VIII	0.37	Smooth	Kevlar	3981	42.41	12.08
30	5	AE	0.37	Smooth	Kevlar	4795	131.38	10.07
31	5	T-VIII	0.5	Smooth	Nylon	3885	88.13	11.60
32	2 ^a	AE	0.5	Smooth	Nylon	4951	97.58	10.25
33	3 ^a	T-VIII	0.5	Smooth	Teflon	4239	125.30	12.08
34	3 ^a	AE	0.5	Smooth	Teflon	4996	14.00	10.29

^aLimited availability of material prevented a full test set of five specimens.

Ratios of the polymer-sheathed bend test results divided by the straight-pull test results (for each material) were calculated and are listed in column G of Table 4. Similarly, strength ratios for the polymer-sheathed specimens relative to the cotton-sheathed specimens are shown in column H of Table 4.

It is observed from these data that performance improvements over the standard cotton sheath were only achieved in two cases (test sets 27 and 33). In both cases, the improvements were observed in T-VIII lines bent over the 0.500-in-diameter smooth bend plate. Kevlar and Teflon sheaths only showed a minor improvement over the standard cotton sheaths (6% and 4%, respectively). In all other test cases, performance was either equal to or less effective than cotton-sheathed static lines.

Table 4. Performance of various sheathing materials compared to the standard cotton sheaths.

Strength Ratios for Polymer-Based Sheathing Materials							
A	B	C	D	E	F	G	H
Test Set	Specimens (count)	Material	Plate Dia. (in)	Surface	Sheathing	P/Straight	P/Cotton
27	5	T-VIII	0.5	Smooth	Kevlar	0.98	1.06
28	5	AE	0.5	Smooth	Kevlar	0.88	1.00
29	5	T-VIII	0.37	Smooth	Kevlar	0.90	0.98
30	5	AE	0.37	Smooth	Kevlar	0.85	1.00
31	5	T-VIII	0.5	Smooth	Nylon	0.88	0.95
32	2 ^a	AE	0.5	Smooth	Nylon	0.87	0.99
33	3 ^a	T-VIII	0.5	Smooth	Teflon	0.95	1.04
34	3 ^a	AE	0.5	Smooth	Teflon	0.88	0.99

^aLimited availability of material prevented a full test set of five specimens.

6.3 Effect of Twists in a Static Line

Additional bend tests were performed to evaluate the effect of the number of twists in a static line. Twist tests were performed with the 0.500-in bend plate on both static line materials. Figure 17 illustrates a single twist test being performed on a T-VIII static line in the bend fixture. The results obtained from these tests are reported in Table 5. Twist numbers referred to in the table indicate the whole number (integer) of 360° twists in the line. For the single (one twist) and double (two twist) tests, the twists were located between the upper grip and the bend plate. The quadruple twist tests consisted of a double clockwise twist above the bend plate and a clockwise double twist below the bend plate.

Figure 18 summarizes the rupture strengths as a function of the number of twists in a line. Most of the reduction of strength occurs as a consequence of the first twist. The sensitivity to additional twists is not as severe. It can be seen that a substantial reduction in strength (about 35%) results from single twisting the T-VIII material, and an 18% reduction is observed for single twisting the AbsorbEdge.

6.4 Effect of Retained Water Tests

Another series of bend tests was performed to investigate the effect of retained water in static lines. A quantity of T-VIII and AbsorbEdge webbing material was immersed in a tank of distilled and deionized water for a period of ~14 days. The material was removed from the tank and allowed to drip dry for approximately one day prior to testing. Water content was noticeable during testing as significant amounts of droplets were released from the material as it was pulled over the bend plate.

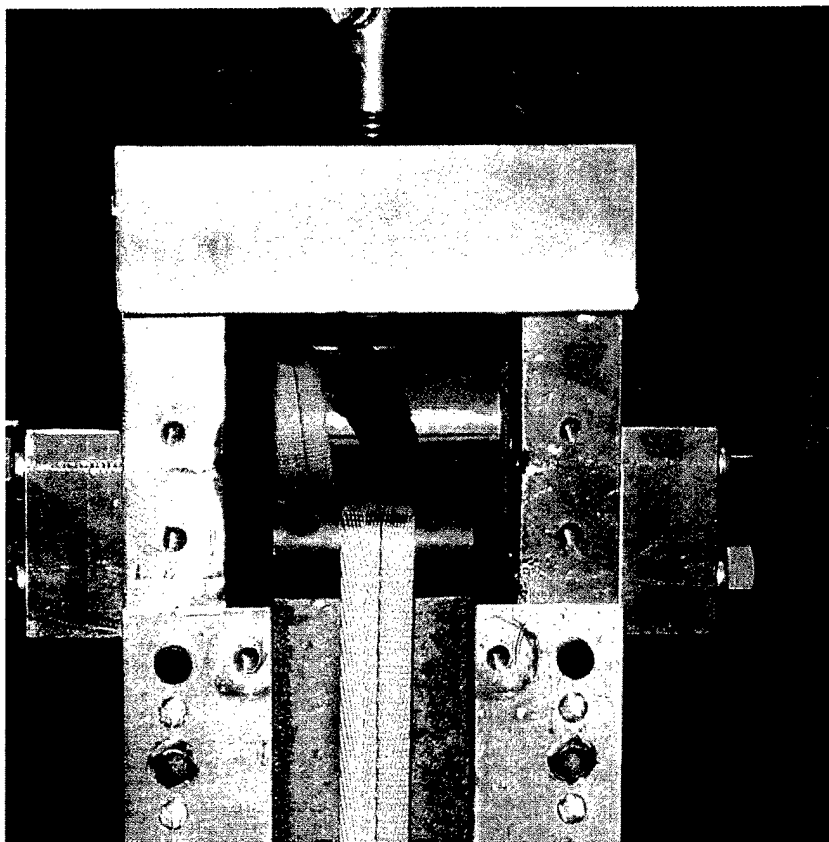


Figure 17. A T-VIII static line with a single twist loaded in the bend test fixture.

Table 5. Test results for twisted static lines.

Rupture Load as a Function of the Number of Twists in a Specimen								
A	B	C	D	E	F	G	H	I
Test Set	Specimens (count)	Material	Pin Dia. (in)	Pin Surface	Sheathing	Twist (count)	Rupture Load	P/Straight
35	5	T-VIII	0.5	Smooth	NA	1 ^a	2803	0.65
36	5	AE	0.5	Smooth	NA	1 ^a	4233	0.83
37	5	T-VIII	0.5	Smooth	NA	2 ^b	2750	0.64
38	5	AE	0.5	Smooth	NA	2 ^b	4119	0.81
39	5	T-VIII	0.5	Smooth	NA	4 ^c	2705	0.63
40	5	AE	0.5	Smooth	NA	4 ^c	4114	0.81

^aSingle twist = 0.0749 revolutions/in.

^bDouble twist = 0.1497 revolutions/in.

^cQuadruple twist = 0.1497 revolutions/in upper; 0.1951 revolutions/in lower.

The test results are summarized in Table 6 and Figure 19. The dry results for the same bend conditions and a ratio of wet-to-dry performance were calculated and reported in column G.

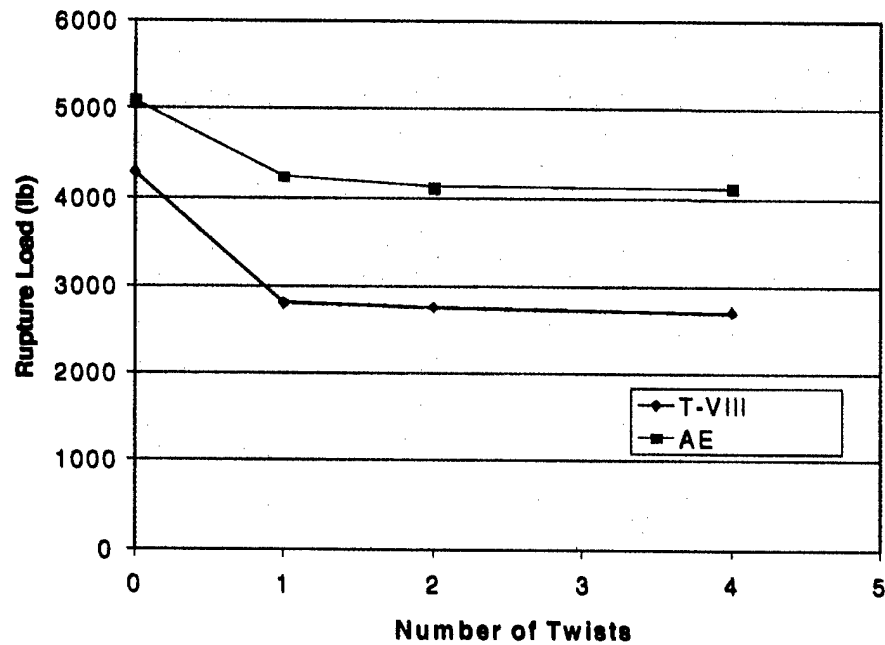


Figure 18. Rupture strength as a function of the number of twists in a line.

Table 6. Results of wet static line bend tests.

Wet Bend Test Results							
A	B	C	D	E	F	G	H
Test Set	Specimens (count)	Material	Bend Diameter (in)	Wet Load (lb)	Dry Load (lb)	Wet/Dry Ratio	Texture
41	5	T-VIII	0.375	2813	2682	1.05	Smooth
42	5	AE	0.375	3872	3985	0.97	Smooth

By observation of data presented in Table 6 and illustrated in Figure 19, it is noted that a slight improvement in strength for the T-VIII material (~5%) was achieved as a consequence of retained water in the webbing material. This phenomenon is most likely the result of the water functioning as a lubricant when the line material slides over the bend plate. An insignificant reduction of strength (~3%) was observed in the case of the AbsorbEdge material tested under identical conditions. In these tests, the AbsorbEdge material reported higher rupture strengths than the T-VIII but demonstrated a degradation in strength compared to its dry load-bearing capacity. T-VIII material, while inherently the weaker of the two, demonstrated a marginal strength improvement.

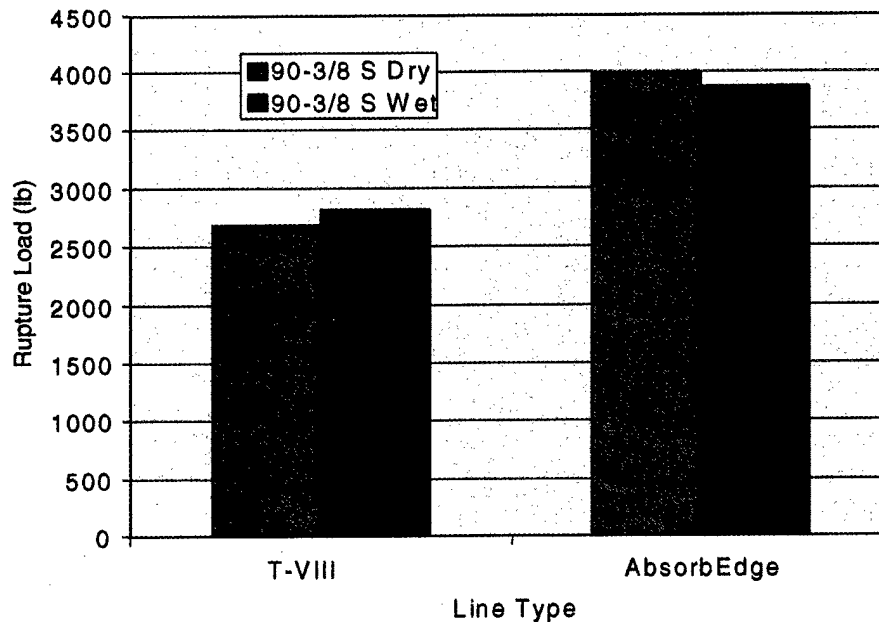


Figure 19. Bar graph illustrating results extracted from Table 6.

6.5 Preconditioned Static Line Tests

The last variable to be evaluated with the bend fixture was the effect of preconditioning, or fatiguing, static line material to determine the degree to which strength is reduced as a consequence of service applications. Based on procurement data, the average number of service applications for a T-VIII static line system is 12 jumps. This figure was determined by calculating the ratio of the number of jumps performed divided by the number of systems procured in any given year (for the past few years).

Static line system inspections tend to be conservative due to the nature of the line's intended function. A value of 50 service applications (jumps) was considered an "extreme" service life and suitable to demonstrate a possible degradation of strength. Consequently, the preconditioning service simulation load was set at 50 cycles of 400 lb/cycle loaded and unloaded at a rate of 40 in/min. The magnitude of the load for a single cycle was determined by attempting to simulate the average parachute deployment load (tensile force to activate deployment) of 400 lb.

Table 7 summarizes the preconditioned test results and includes the unused (manufacturer supplied) results for similar conditions. The strength loss is shown graphically in Figure 20. In the straight-pull configuration, the strengths were reduced by the conditioning about 6% and 11% for the T-VIII and AbsorbEdge lines, respectively. However, in the bend tests the effect of this conditioning on rupture strength was negligible.

Table 7. Test results for preconditioned static line material.

Test Results for Preconditioned Static Line Material								
A	B	C	D	E	F	G	H	I
Test Set	Specimens (count)	Material	Pin Dia. (in)	Pin Surface	Load History (No. Cycles/lb)	Rupture Load (lb)	Unused Capacity (lb)	Fatigued/Unused Ratio
43	5	T-VIII	NA	NA/Straight	50/400	4177	4438	0.9412
44	5	AE	NA	NA/Straight	50/400	5055	5667	0.8920
45	5	T-VIII	0.370	Smooth	50/400	2552	2682	0.9515
46	5	AE	0.370	Smooth	50/400	3997	3985	1.0030

Note: NA = Not applicable.

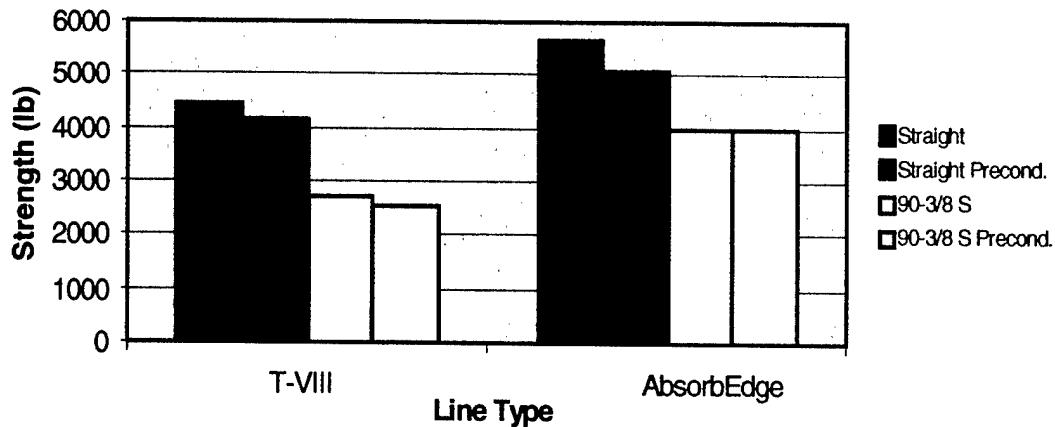


Figure 20. Strengths of fatigue conditioned T-VIII and AbsorbEdge static lines compared to unused materials in both straight-pull and bend-plate configurations.

A graph of the preconditioning load history was plotted and demonstrates the accumulated "plastic" strain encountered during the cycling process. The cycling history plot for a section of T-VIII webbing material is presented in Figure 21. The plot is representative of the preconditioning cycle used to precondition both the T-VIII and AbsorbEdge test specimens. Loads averaged ~400 lb for 50 consecutive cycles (cycling occasions).

Figure 21 clearly shows a significant amount of increased plastic strain as a function of the number of loading cycles. Some of this effect was expected, as a significant amount of plastic (nonrecovering) elongation is the result of straightening out the weave in the textile's tows (bundles of fibers). This straightening can be readily observed in the difference in slopes of the first two cycles. Cycle 1 began at a load of 50 lb, loaded to 400 lb, and then decreased to 0 load to begin cycle 2 (at 0 lb). The loads of the return strokes are not included in this data. (A preload of 50 lb was used to hold the static lines firmly in the grips to begin testing. This was done for all preconditioning cycles.) Notice that

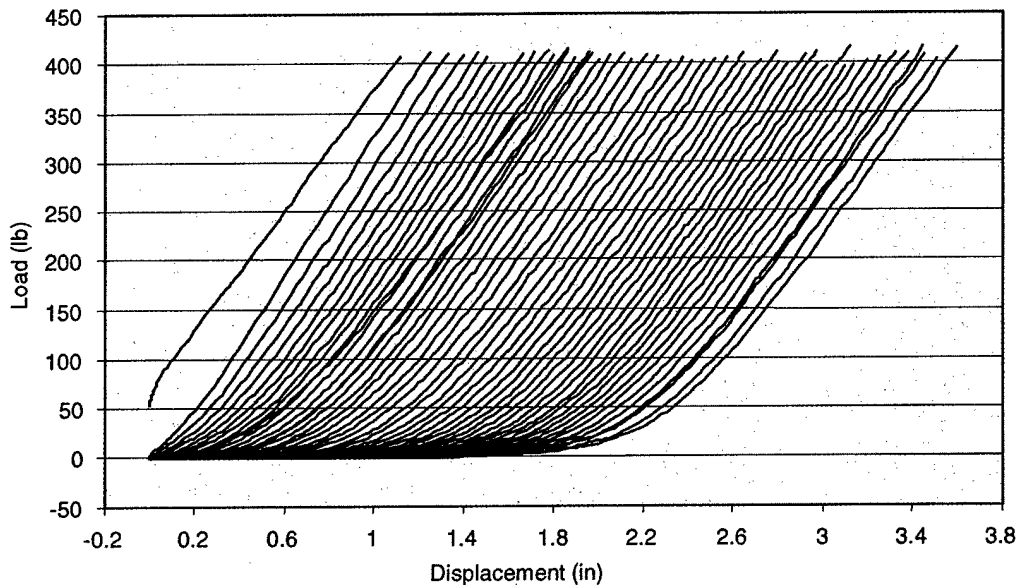


Figure 21. Precondition loading history, shown as load vs. displacement for a T-VIII web.

the slope of cycle 2 for loads over 100 lb (~ 354 lb/in) is greater than the slope of cycle 1 for loads above 100 lb (~ 306 lb/in). As the fibers and weave are pulled into the axis of the load, the static line becomes stiffer. Stiffening is also observed within each cycle as the change in slope during the cycle. As the cycles continue, there is a shift of about 2.2 in from the displacement to produce a given load from the second cycle to the last. It is unknown, however, what portion of the plastic set is the result of actually drawing the individual nylon fibers and what portion is due to textile weave straightening.

During the cycling process, test operators observed the progression of slack being generated as the number of cycles increased. The test machine was set to the "load control" mode, and the crosshead returned to the "zero" load position between each cycle. The progressive elongation resulted in the loss of contact with the bend plate after a moderate number of cycles. Successive cycling resulted in the advancement of the location of contact between the test specimen and the bend plate. Contact position advancement was contained to within a length of ~ 1.25 in. This change in contact position was considered an acceptable variance because an actual line would contact the door edge at slightly different locations throughout its service life.

6.6 High-Speed Video Observation of Rupture Events

High-speed video was taken of both the T-VIII and AbsorbEdge static lines in the bend fixture at a rate of 2000 frames/s with a shutter speed of $23 \mu\text{s}$. Figure 21 shows the front view of a T-VIII static line bearing on a 0.500-in smooth bend

plate mounted in the bend fixture. A similar experiment for AbsorbEdge is shown in Figure 22. The figures show (from left to right) two consecutive frames taken prior to failure and one frame taken after failure. A total of 11 tests were videotaped in this manner from three views—top, bottom, and front—simultaneously.

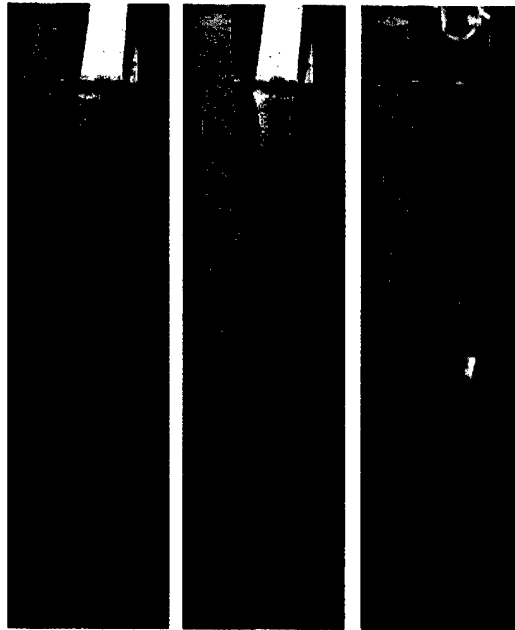


Figure 22. High-speed video frames of a T-VIII static line during rupture.

Of particular interest in both of these figures is the rate at which necking accelerated just prior to failure. Both figures show an even distribution of longitudinal strain $1/1000$ th of 1 s (two frames) prior to failure (based on the edges of each line being parallel near the failure zone). At one-half that time ($1/2000$ th of 1 s, middle frames), excessive necking in both materials is observed. Catastrophic failure occurred in both lines in less than $1/2000$ th of 1 s after the necking was photographically observed. The blurring of the image in the third frame gives an indication of the speed at which the static line breaks and releases strain energy. In all cases, a loud noise is heard when the static lines fail in the fixture with failures in smooth bend configurations, somewhat louder than rough bends. With a known crosshead displacement rate of 40 in/min, a $1/2000$ th of 1 s interval equates to a longitudinal travel (crosshead displacement) of 3.3×10^{-4} in.

Transversely oriented green pen marks (Figures 22 and 23) had initially been drawn on the specimens at 1-in intervals (with no applied load). Textile straining is confirmed by observing the position of the green pen mark in the video frames. Just prior to failure, the marks have advanced from their initial



Figure 23. High-speed video of an AbsorbEdge static line during rupture.

1-in spacing to an additional 25–30% (approximately). These observations are consistent with macroscopic strain to failure capacities of the static line material and show that the T-VIII material exhibits a greater capacity for strain to failure.

Pen marks close to and far from the bend plate do not appear similar. A noticeable characteristic of pen marks close to the bend plate is their non-straight and non-parallel shape observed on both materials. In the AbsorbEdge material, the shapes of the marks close to the bend plate appear symmetric about the longitudinal centerline of the specimen and spread from the centerline in a chevron pattern. In the T-VIII material, no distinct pattern appears other than a noticeable translation of one top web relative to the other resulting in a discontinuity at the web seam. These changes are indicative of uneven strains close to the bend plate where the fiber strains are not uniformly distributed across the width of the web.

It is obvious that at locations close to the bend plate, strains are manifested in both textile stretching and in unevenly distributed fiber straining. Far from the bend plate, elongation seems limited to an evenly distributed textile elongation only.

7. Web Construction and Failure Characteristics

Still photographs and high-speed video frames were used as an aid to contrast the differences in failure characteristics of the two types of static line material. It was suspected that the “rolled and sewn” construction of the T-VIII material

contributes to an uneven distribution of load between the upper and lower webs when tested in the bend configuration. Figure 24 shows a schematic of the T-VIII static line rolled and sewn webbing construction.

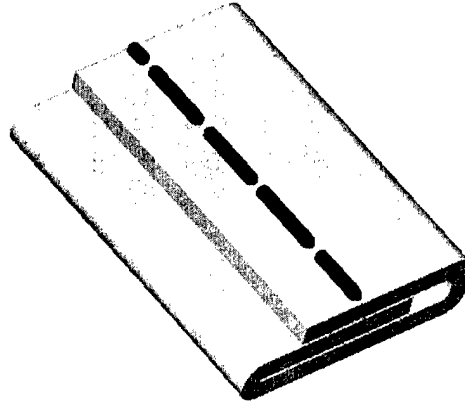


Figure 24. Schematic of the T-VIII static line rolled and sewn webbing construction shown "seam side" up.

Observing the details shown in Figure 24, it is noted that the T-VIII static line is constructed from a single thin layer of woven nylon folded over twice to overlap along the centerline where it is transversely stitched through all three layers. The construction process results in a pair of parallel tubes with a three-layer accumulation of webs along the centerline. The color-coded nylon stitching (shown in black in the figure) is applied to maintain the cross-sectional configuration of the line.

Figure 25 shows a schematic of the AbsorbEdge construction. The AbsorbEdge design also features a dual tubular cross section but differs from the T-VIII design in that the tubes result from transversely stitching through the centerline of a single woven tube (as opposed to folding over a single flat web as is done in T-VIII line construction). Another distinct difference contrasting the two designs is that the AbsorbEdge webbing incorporates longitudinally oriented nylon tows built into the tubes to aid in supporting tensile loads. These tows are shown in Figure 25 and are represented by the blue cylindrical shaped extrusions extending from the tubes.

A unique feature of the AbsorbEdge design is the symmetric cross section that aids in maintaining a midplane neutral axis through severe 90° bends. Conversely, the T-VIII webbing is not symmetric and varies in layer count from two layers along each edge to three overlapped layers at the center. The T-VIII rolled and sewn construction technique results in a non-midplane neutral axis while in a bent configuration.

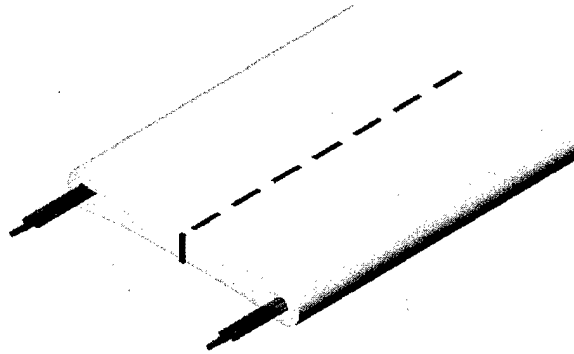


Figure 25. Schematic of the AbsorbEdge static line webbing construction, including longitudinally oriented tows of nylon shown in blue.

Load-displacement curves generated during bend testing feature characteristics unique to each type of line material. The T-VIII material produced smooth uniform plots up to failure for (all non-sheathed) straight-pull, the 0.500-in-diameter smooth bend, and from all the rough bend tests. The 0.375-in and 0.250-in smooth bend tests resulted in the last 1–1.5 in of crosshead displacement exhibiting raggedness due to partial failures and subsequent line or web reloading. The sequential web failures/reloading pattern results in uneven tensile loads across the width of the line and therefore caused in-plane shearing of the textile weave. The magnitude of uneven loading can be sufficient enough to break the transverse stitching thereby permitting noneven web translations resulting in a repositioned instantaneous load path. On occasion, the nonuniform web translations resulted in the failure of the black transverse stitching with smooth bend plates. This is likely the result of the folded over webs on the top of the line translating at a faster rate than the web in contact with the bend plate.

Figure 26 shows a T-VIII line loaded in the bend fixture with a 0.500-in rough bend plate. Figure 27 shows another T-VIII line loaded with a 0.375-in rough bend plate. In both figures, evidence of torn transverse stitching is shown (Figure 26 shown tearing just prior to contact at the bend plate; Figure 27 shows tearing after the bend plate). Also evident is the pattern of shear loading as manifested by the obvious diagonal patterns assumed by the right-hand side of the textile web.

The crisp failure features of the load-displacement curves attained with the T-VIII material using rough bend plates are likely due to catastrophic failures initiated by excessive tearing damage imparted by the surface of the knurled bend plate. In these test cases, it is likely that the rough surface of the bend plate evenly retarded translation of the lower web of the specimen and prevented shear transfer of tensile loads. In this configuration, a failure would be catastrophic as is shown by the sharp clean failures plotted on the rough bend load-displacement curves (with 0.500-in rough bend being the single exception).



Figure 26. Failure region of the load-displacement curve for both materials using 0.500-in-diameter rough bend plate.



Figure 27. T-VIII specimen with 0.375-in-diameter rough bend plate. The absence of the transverse stitching is shown below the bend plate.

Contrasting this behavior are the plots generated with AbsorbEdge static lines. Smooth load-displacement plots were generated with AbsorbEdge specimens in the straight-pull and smooth bend tests (with a single specimen as an exception) but were not produced during the rough bend tests. Ragged plots indicating failures and reloading of fiber groups were produced for virtually all AbsorbEdge rough bend (non-sheathed) tests.

Figure 28 details the characteristics of the pre-failure load-displacement behavior of both static line types tested in the straight-pull configuration. The full array of non-sheathed bend-pull configurations, with both smooth and rough bend plates and with all three bend diameters are shown in Figures 29–34.

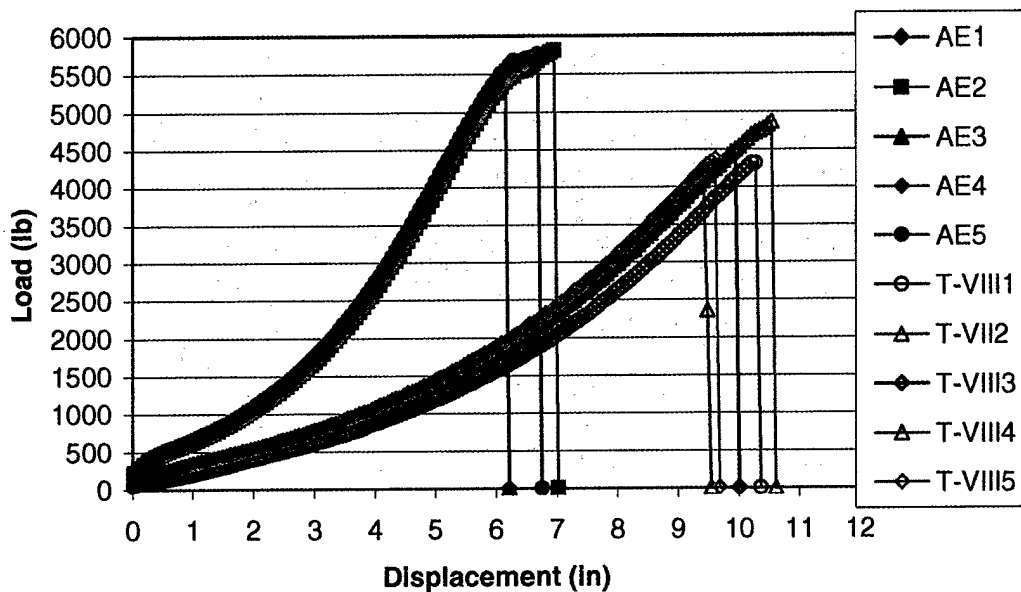


Figure 28. Load-displacement curves generated for T-VIII and AbsorbEdge specimens in the straight-pull configuration.

Based on these observations, it was suspected that the bearing web of the T-VIII specimens tended to resist translation over the smooth bend plates while the upper webs continued to translate over the bend. This behavior would result in load shifts from quasi-evenly distributed loads through the static line thickness, to uneven (top vs. bottom) web loading. Excessive web strains would result from the constrained motion of the lower web while negotiating the sharp angle bends encountered in the fixture. Strain to failure due to these circumstances could be prematurely achieved. Figures 35 and 36 show evidence to support this theory.

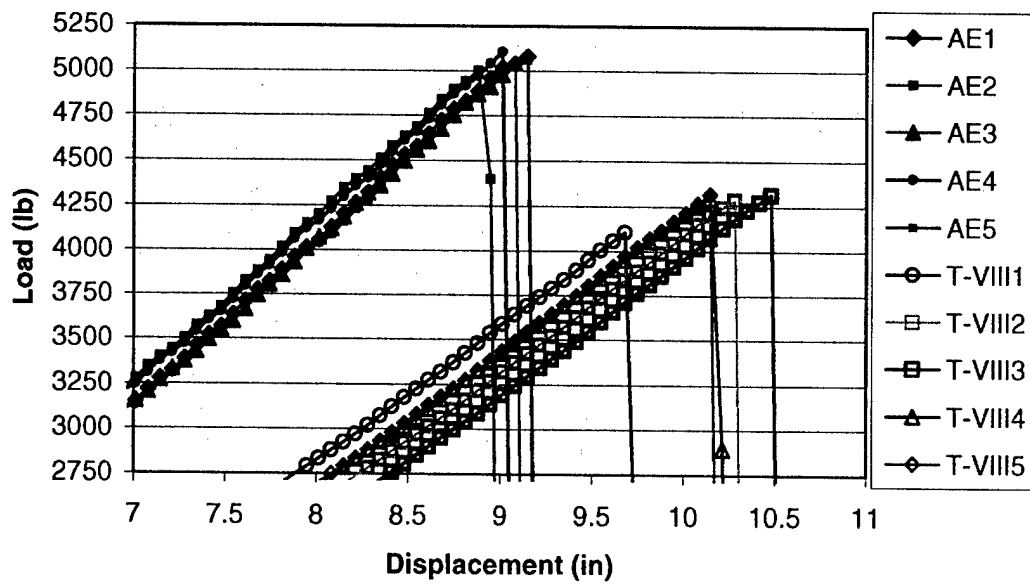


Figure 29. Failure region of the load-displacement curve for both materials using 0.500-in-diameter smooth bend plate.

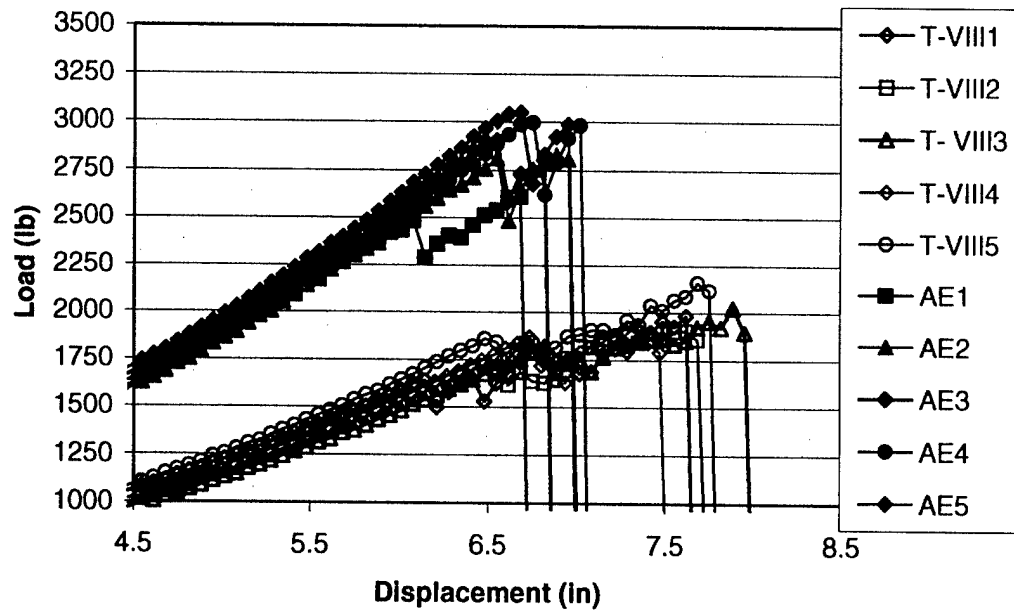


Figure 30. Failure region of the load-displacement curve for both materials using 0.500-in-diameter rough bend plate.

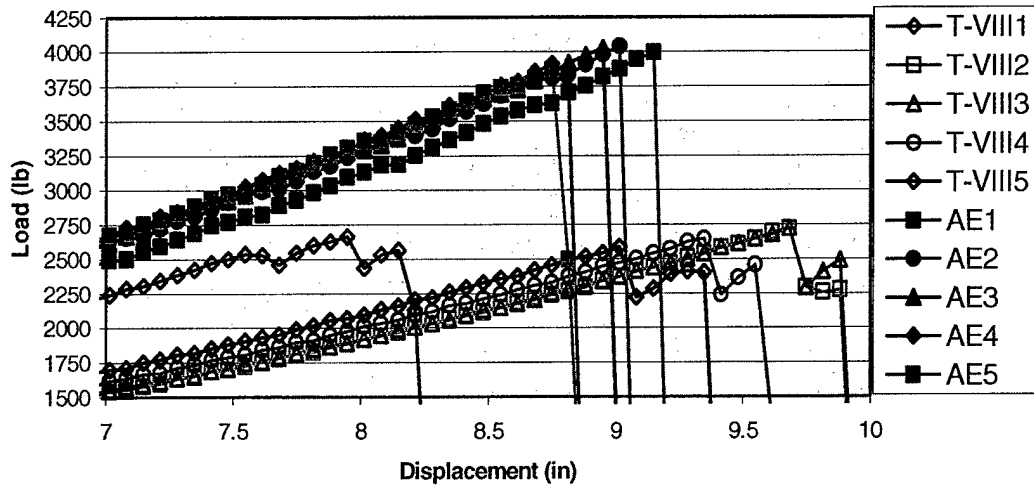


Figure 31. Failure region of the load-displacement curve for both materials using 0.375-in-diameter smooth bend plate.

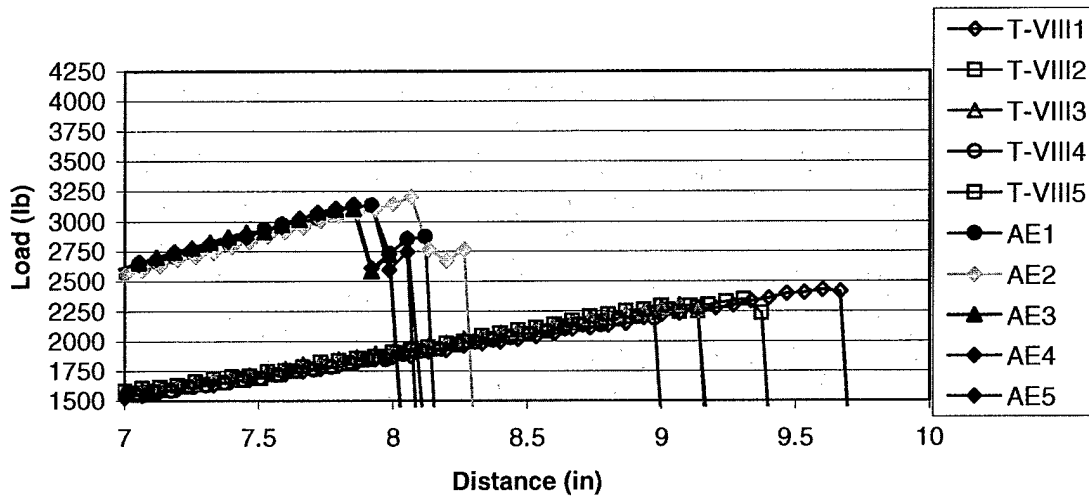


Figure 32. Failure region of the load-displacement curve for both materials using 0.370-in-diameter rough bend plate.

Figure 35 shows the AbsorbEdge load vs. displacement curves generated during test set 2 (straight-pull) and test set 8 (0.500-in rough bend). Notice that the average spring constant (the average slope of the curves) for the straight-pull tests is significantly higher than the spring constant obtained from the bend test curves. The displacement to failure, however, is about the same for the

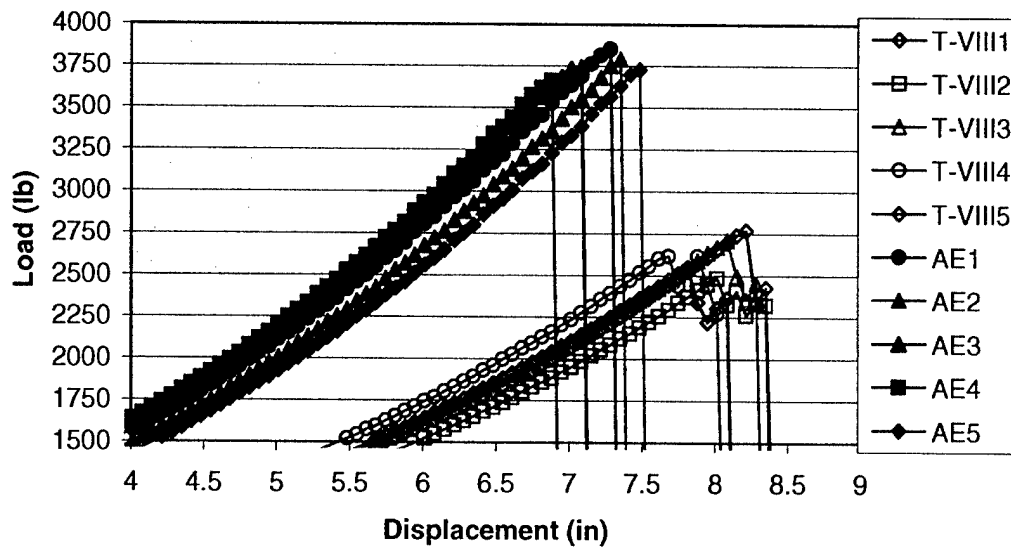


Figure 33. Failure region of the load-displacement curve for both materials using 0.250-in-diameter smooth bend plate.

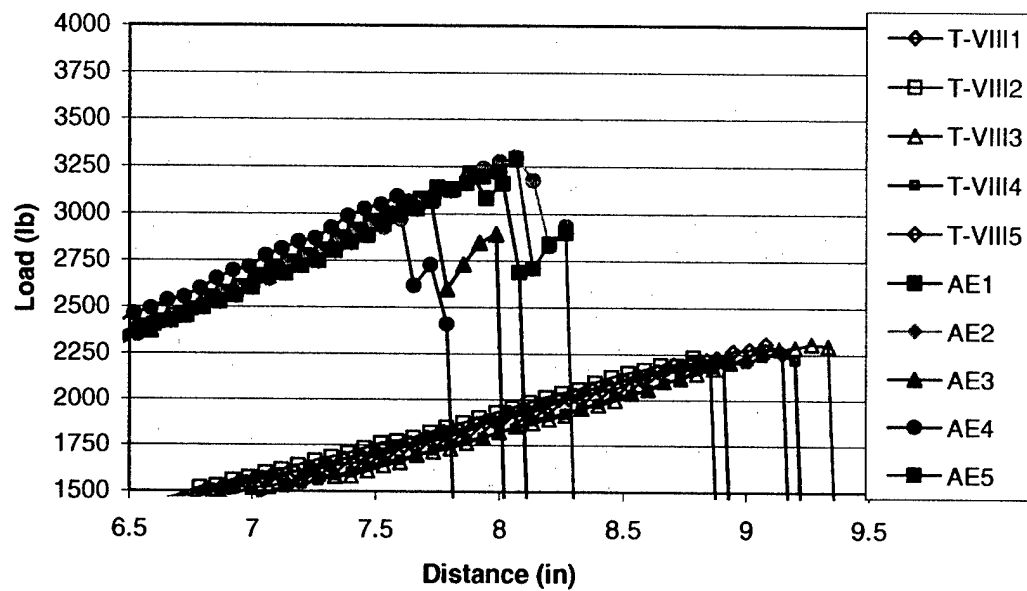


Figure 34. Failure region of the load-displacement curve for both materials using 0.250-in-diameter rough bend plate.

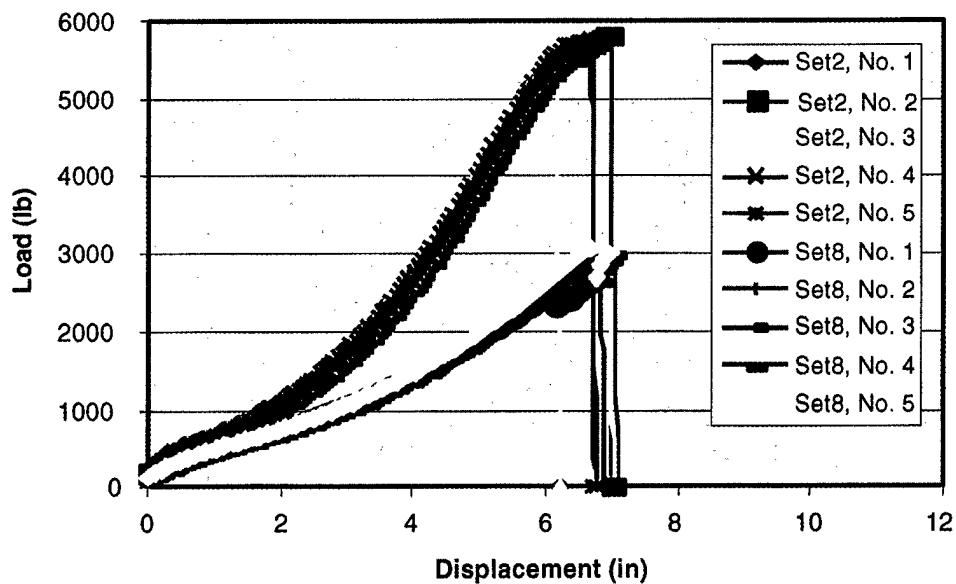


Figure 35. Load-displacement traces of straight vs. rough 0.50-in bend pull for AbsorbEdge.

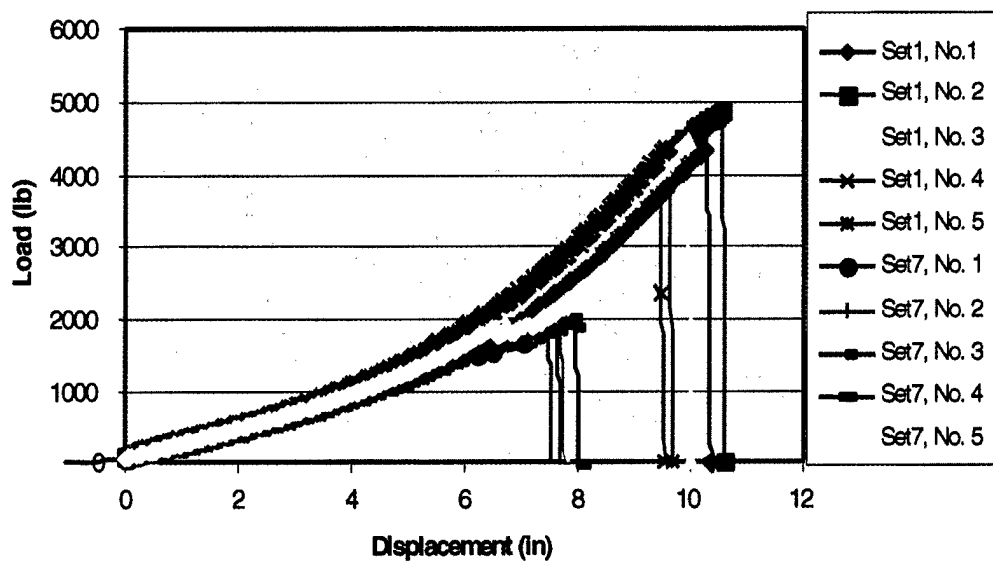


Figure 36. Load-displacement traces of straight vs. rough 0.50-in rough pull for T-VIII.

AbsorbEdge material in the straight-pull and bend configurations. The active gage length of the specimen is considerably longer in the bend test configuration explaining some of the change in the effective stiffness (as loading is achieved by the displacement of the test machine crosshead). The change in load distribution, due to the bearing of the material around the bend plate contributes to the change (reduction) in rupture strength as compared to the straight-pull tests.

Figure 36 shows the curves generated for the T-VIII material (test set 1—straight-pull and set 7—0.500-in rough bend) shown in a format similar to Figure 35. For the T-VIII curve sets, the two spring constants (straight and rough bend) are indistinguishable up to the onset of bend specimen failure. The lower stiffness due to the extended gage length observed with the AbsorbEdge bend specimens is not apparent with the T-VIII. Additionally, a reduction in displacement to failure occurs with the T-VIII between the straight-pull and bend-pull tests unlike the response seen in the AbsorbEdge comparison.

Additionally, the T-VIII bend specimens exhibits a region of about 2 in of displacement (between the 6- and 8-in ticks along the abscissa of Figure 36) where the specimens from test set 7 appears to soften prior to failure. Transversely oriented fibers drawn over the abrasive surface of the knurled plates are probably damaged (and eliminated from transferring any portion of a shear load), which results in a lengthening of the specimen or gage length. Since the loads are applied by displacement of the crosshead of the test machine, an instantaneous lengthening of a gage length results in a load drop as shown for all test set 7 specimens.

8. Validation of Uneven Web Translations

To confirm the suspicions of uneven web translations over bend plates, a series of tests were performed using ordinary steel shirt pins inserted through the webs of each type of specimen. The pins were placed in transversely oriented rows of four at ~1-in intervals along the specimens. The intent was to detect any change in the angular orientation of the pins as they advanced towards the bend plate. Pins inclining forward (toward the bend plate) would indicate accelerated upper web straining. Pins inclining away from the direction of elongation would indicate accelerated lower web straining.

Figure 37 shows both the T-VIII (lower specimen [b] and the AbsorbEdge (upper specimen [a]) static lines prepared with the series of pins arranged in parallel rows spaced 1 in apart (along the green pen marks).

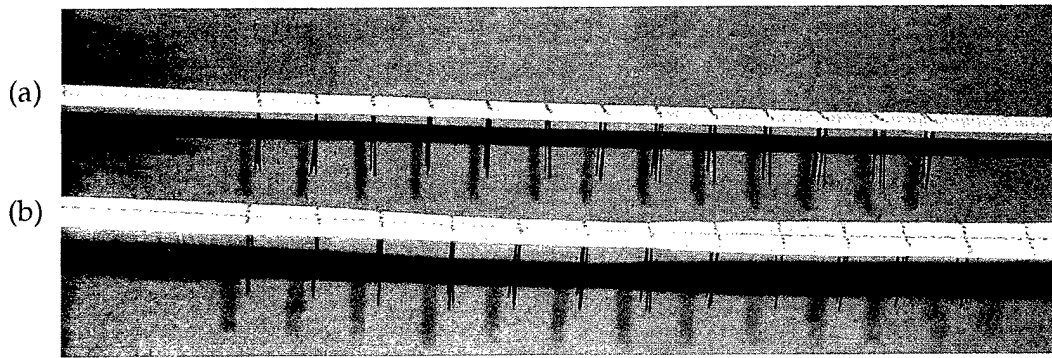


Figure 37. Unloaded specimens prepared with rows of perpendicularly oriented pins.

Figure 38 shows both specimens (T-VIII on the left [a] and AbsorbEdge on the right [b]) loaded side by side in the bend fixture using a 0.500-in smooth bend plate subjected to a shared load of ~185 lb.

The pins shown in Figure 38 were virtually perpendicular to the upper web surface of the test specimens subject to a preload of ~185 lb. As loading progressed, the rows of pins advanced toward the bend plate and began to

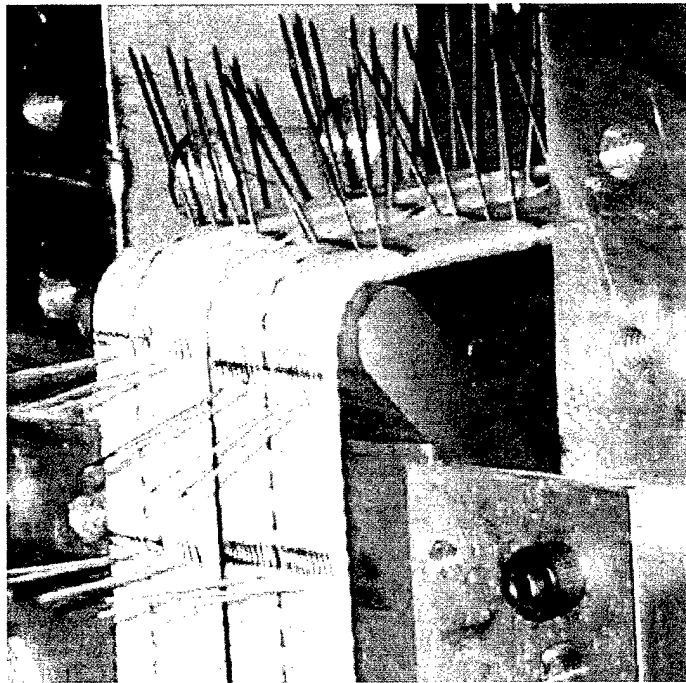


Figure 38. Bend fixture with a 0.500-in smooth bend plate, (a) T-VIII and (b) AbsorbEdge.

incline forward as shown in Figure 39 (~2100 lb). The orientation of inclined pins is indicative of the upper web straining (translating) at a greater rate than the lower web and proves the difference in their relative motions.

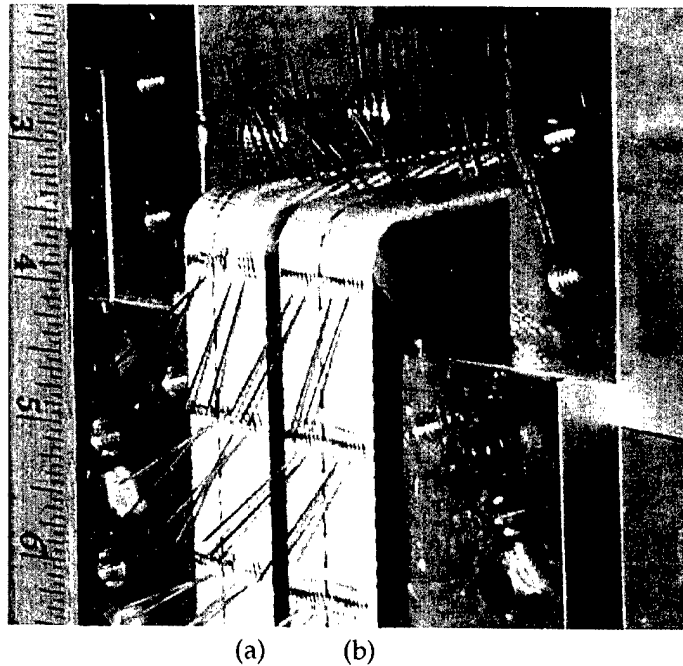


Figure 39. Bend fixture with a 0.500-in-diameter smooth bend plate loaded to ~ 2100 lb, (a) T-VIII and (b) AbsorbEdge.

Of equal significance is the orientation of the inclined pins after (below) the bend plate. Figure 39 shows three rows of inclined pins after having been pulled over the bend plate. All of these pins exhibit the advanced upper web orientation. The only noticeable difference is that the T-VIII specimen shows the second pin from the left (positioned through all three layers) at a lesser incline than adjacent pins for each of the rows shown (pre- and postbend plate). This behavior indicates the difference in translation rates across the width of the T-VIII line. The AbsorbEdge line shows a more consistent pattern of even inclines across the width of the specimen for each of the pin rows.

A selection of three consecutive high-speed video stills is shown in Figure 40, where a single T-VIII specimen is being tested in the bend fixture. The inclined orientation of the pins is evident both before and after the bend. This would imply, as is also the case with AbsorbEdge, that the upper web pulls material from the upper (horizontal) portion of the specimen (as part of the elongation process) long before contact with the bend plate.

(a)



(b)



(c)

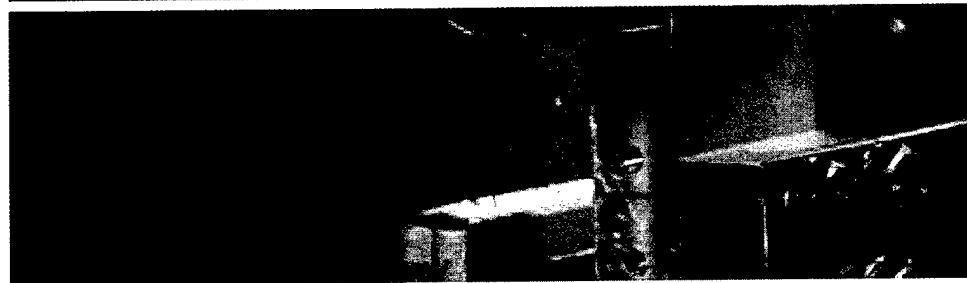


Figure 40. Photographic record of the pin-test for T-VIII webbing (a) 20 s prior to failure, (b) 15 s prior to failure, and (c) 0.0010 s prior to failure.

9. Test Data Summary

Data collected from the various tensile tests performed during this investigation clearly demonstrate that the AbsorbEdge webbing material outperforms the standard T-VIII for all types of straight and bend plate rupture tests. A summary of these results is presented in Table 8 and Figure 41. Table 8 summarizes the percent improvement in rupture strength AbsorbEdge webbing material offers over the standard T-VIII. For convenience, the general test parameters are presented in various columns with the percent calculation (AbsorbEdge relative to T-VIII) shown in the last column. A graphical summary of the raw strength data for all of the test conditions reported herein is shown in Figure 41. For the straight-pull tests, the AbsorbEdge webbing demonstrated a 27.6% increase in strength over the standard T-VIII webbing structure.

Table 8. Percent improvement of AbsorbEdge compared to T-VIII for various tests conditions.

Percent Improvement of AbsorbEdge Compared to T-VIII					
Test Type	Bend Plate	Condition	T-VIII (lb)	AbsorbEdge (lb)	% Improved (AbsorbEdge to T-VIII)
Standard Bend	0.500 Smooth	Nonsheathed	4285	5089	19
Standard Bend	0.370 Smooth	Nonsheathed	2452	3985	63
Standard Bend	0.250 Smooth	Nonsheathed	2410	3772	57
Standard Bend	0.500 Rough	Nonsheathed	1989	2846	43
Standard Bend	0.370 Rough	Nonsheathed	2317	2824	22
Standard Bend	0.250 Rough	Nonsheathed	2266	2882	27
Standard Bend	0.500 Smooth	Cotton	4082	5024	23
Standard Bend	0.370 Smooth	Cotton	4073	4795	18
Standard Bend	0.250 Smooth	Cotton	3147	4448	41
Standard Bend	0.500 Rough	Cotton	4324	5065	17
Standard Bend	0.370 Rough	Cotton	4120	4996	21
Standard Bend	0.250 Rough	Cotton	3997	4725	18
Poly-Sheathed	0.370 Smooth	Kevlar	3981	4795	20
Poly-Sheathed	0.500 Smooth	Nylon	3885	4951	27
Poly-Sheathed	0.500 Smooth	Teflon	4239	4996	18
Preconditioned	Straight	Nonsheathed	4177	5055	21
Preconditioned	0.370 Smooth	Nonsheathed	2552	3997	57
Wet	0.370 Smooth	Wet/Nonsheathed	2813	3872	38

Both materials exhibited sensitivity trends of decreasing strength with decreasing smooth-bend plate diameters. These trends were observed in both the sheathed and non-sheathed smooth bend plate test configurations (with the single notable exception of the T-VIII material with the 0.500-in smooth plate, a suspect outlier).

Standard cotton sheathing proved successful in increasing the rupture strength in all (smooth and rough) bend test configuration without violating established strength vs. bend diameter trends (again, with the single notable exception of the T-VIII material with the 0.500-in smooth plate).

Severe strength reductions were observed in both non-sheathed materials when tested with the rough bend plates. Rough textured bend plates exacerbated the effect of friction and caused premature damage to the specimens. Trends of decreasing strength with decreasing bend diameter were virtually reversed in the non-sheathed rough plate bend tests.

Polymer-based sheathing material did not afford significant advantages to either material when compared to the standard cotton sheaths. Slight advantages were obtained in some applications of polymer-based sheaths, but trends in improvements were not consistent. This would imply that protection of from direct contact with the bend plate (door edge) would be advantageous

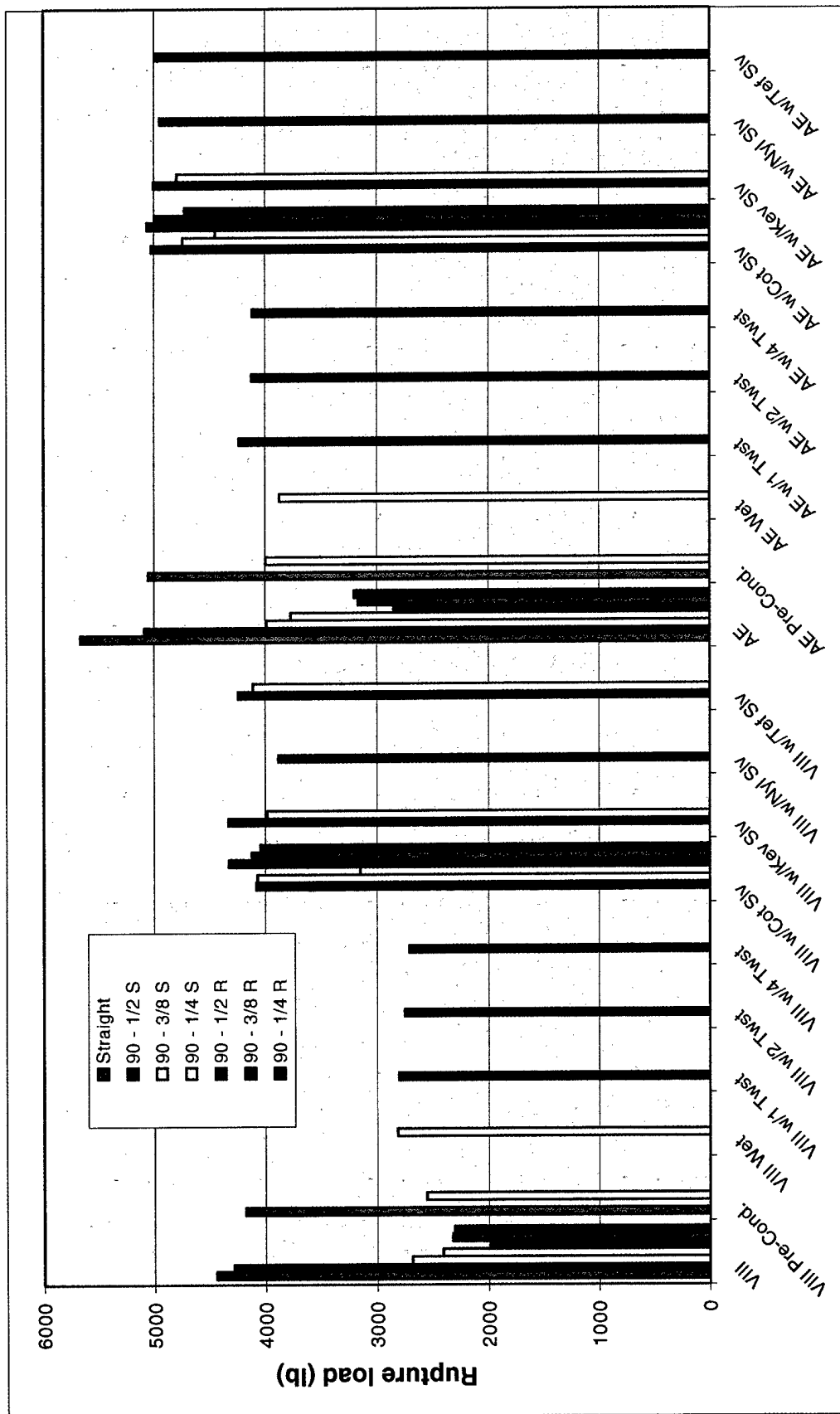


Figure 41. Average specimen strength for various test conditions for both AbsorbEdge and T-VIII nylon webbing.

regardless of which sheathing material is applied. The choice of which material to use would most likely reduce to issues related to economics, manufacturability, maintainability, and life cycle.

Trends of strength vs. the number of twists in a static line were determined for both materials. It was observed that a single twist over the 0.500-in smooth bend plate reduced the strength of the T-VIII material by ~35%. Similar test conditions reduced the AbsorbEdge strength by ~18%. Additional twists showed no significant effect on either material.

Tests performed to determine the sensitivity of both materials to retained water showed relatively insignificant changes in strengths. The T-VIII material showed an increase in strength of ~5%. AbsorbEdge results showed a decrease in strength of ~3%. While the changes in rupture strengths are minor, it is interesting to note that the effects of retained water on the two types of webbing material are opposite. For the T-VIII material, water functioned as a lubricant, and its benefits outweighed the disadvantages associated with decayed (from moisture absorption) material properties (a known attribute of nylon). The AbsorbEdge material behaved more like monolithic nylon and showed a predictable decrease in strength from having been immersed in water.

Preconditioning tests were performed to determine the sensitivity of the webbing materials to service fatigue. Trends of decreasing strength as a function of increased service applications were apparent for both materials in the straight-pull tests. T-VIII material exhibited a loss in strength of ~6%, while AbsorbEdge showed an approximate 10% loss. There were smaller losses due to preconditioning seen in the bend tests. The AbsorbEdge, while seemingly more sensitive to fatigue, still reported higher rupture strengths after preconditioning than did the standard T-VIII.

Pin tests performed on both materials confirmed the theory that the web translation rates differ between the upper and lower webs while loaded in the bend fixture. The rolled and sewn construction of the T-VIII line seems to show a higher degree of sensitivity to bending, which is routinely manifested in uneven straining across the width of the line. It is also likely that the ragged pre-failure load-displacement curves generated for the T-VIII material using smooth bend plates is yet another manifestation of the uneven web translations (caused by individual load path failures occurring in highly loaded webs which consequently cause amplification of loads in the lesser loaded webs).

10. Conclusions and Recommendations for Future Work

Two of the most influential factors contributing to the reduction of static line strength are the bend radius and the contact surface roughness. For all bend test configurations performed in this study, the addition of a standard cotton sheath

increased the rupture strength of both materials by significant percentages. For example, it was determined that a smooth radius of 3/16 in reduced the strength of the T-VIII line to 60% of its straight-pull strength (from 4439 to 2683 lb). A rough surface at this radius further reduced the strength to 2323 lb or to 52% of the straight-pull strength. Utilizing a cotton sheath with the same rough surface and radius restored its strength to 4120 lb (93% of straight-pull strength).

The obvious performance improvement achievable with the application of the standard cotton sheath renders this enhancement a potentially quick and inexpensive solution to the problem of premature static line failures. Additional tests are recommended to determine the performance of sheathed static lines subjected to test conditions used to evaluate non-sheathed lines such as twisted-sheathed, wet-sheathed, and preconditioned-sheathed. Performance results obtained from these tests could be used to qualify a sheathed static line system as an immediate upgrade to fielded systems. Further development of the sheathed line system is clearly warranted.

Attempts should also be made to correlate test results generated in this investigation with tests performed at dynamic loading rates and longer (more realistic) specimen lengths. Results from this investigation identified trends of static line strength sensitivity to numerous test variables. However, all tests performed in this investigation were done at quasi-static loading rates on subscale lengths of material. The effects of increased loading rates and active gage lengths on established sensitivity trends are currently unknown. Efforts should be made to integrate the test conditions examined in this report with dynamic load rates, test conditions and specimen lengths examined by Millette et al. [4]. Results from test efforts such as these could demonstrate an amplification or reduction in the existing quasi-static trends.

It is reasonable to theorize that the combined effects of two or more adverse test conditions may be superimposed to reduce the material strengths by a measure commensurate with the sum of the individual effects. An investigation to determine the effect of combined strength reducing conditions may explain how and why random static line failures currently occur in personnel airdrop operations.

In some instances, jumpers may impart a twist to their static line while locking onto the aircraft anchor line or while tumbling outside of the aircraft (tests show a possible 35% strength loss). If that soldier's line has been considerably fatigued (tests show a possible 5% strength loss), and if the aircraft door edge is abraded or rough (tests show as much as 55% strength loss), the combined effects may accumulate to an unacceptable combination of strength reductions. For a T-VIII static line system, these hypothetical values may reduce the rupture strength from 4439 lb in the straight-pull configuration (as determined by these tests) to 28% or 1230 lb $[(1-0.35) * (1-0.05) * (1-0.55)] = 0.28$ or 72% strength reduction. An

examination of the issue previously presented is recommended to determine the effect of accumulated adverse conditions on static line strength retention.

The T-VIII line clearly showed a high degree of sensitivity to contact web friction. It is recommended, particularly due to the dramatic strength reductions observed on rough surfaces, that the effect of which T-VIII web (seamed vs. nonseamed) contacts the bend plate should be investigated. All testing in this investigation was performed with the seam of the T-VIII line positioned away from the bend plate surface. This practice was maintained throughout all tests in an effort to reduce the effects of random variables influencing results. In retrospect, however, this variable is considered a potential contributor to the reduction of the T-VIII line strength. A short series of tests could answer this question.

A transverse sliding bend test, while difficult to perform, may also prove useful in more accurately simulating the motion of a static line over a door edge. Bend tests performed in this study considered elongation only and did not address the transverse sliding motion downwards, along the edge of the door. Effects of friction for this type of motion may contrast the effects determined for the tests reported.

A similar series of bend tests should also be conducted with load-monitoring sensors (load cells) positioned in the grip supports of the bend fixture. Additional data collected from such modifications could demonstrate uneven load distributions along the length of a static line while in contact with a door edge. Evaluation of this data could also aid in the development of new systems featuring integral shock absorbing mechanisms for additional soldier safety.

The development and application of nondestructive testing techniques are recommended for inexpensive Go-/NoGo-type field inspections. Currently, static line inspections are limited to visual methods in which an experienced rigger is expected to make judgments regarding the structural integrity of static line systems. It is obvious that reductions in strength from fatigue and material property degradation from water absorption are not visually detectable. Furthermore, internal damage to the webs and edges of the rolled and sewn T-VIII line may go unnoticed during visual inspections. Therefore, an effort to identify and qualify nondestructive test methods for static line evaluations is suggested. One method commonly used for both polymer and wire rope inspections is acoustic signature monitoring. DSC and routine tensile testing of fleet inventories might also be conducted on random samples judged suitable for service. Test results may indicate flaws in current inspection methods.

Another topic that deserves further investigation is the preconditioning, or fatiguing, of static lines. In this study, only the static lines were preconditioned, static lines with sheathes were not. Preconditioning cycles performed for these tests applied the nominal operating load of 400 lb. Full characterization of

fatigue damage would be more accurate with the inclusion of some higher "anomaly load" cycling.

Finally, in noting the structural design advantages of the AbsorbEdge cross section, and, noting that good energy absorption characteristics reduce transmitted shock, it may prove useful to investigate the performance of an AbsorbEdge design incorporating mechanically deformed tows of longitudinally oriented fibers. This concept would preserve the ultimate strength characteristics of the current AbsorbEdge design while extending the strain to failure limitations. Effectively, this concept would reduce the current spring constant and enhance the elongation characteristics of the material.

Mechanics may also play a part in causing the seemingly random static line failure events. Shock waves travel along strings in accordance with known mathematical relations. Superposition of shock impulses could, under some circumstances accumulate at critical locations in a static line and cause failure. This possibility is currently being examined. Methods to incorporate redundant line systems that would allow a failure of the primary static line load path while still maintaining terminal connections are a possible solution to the problem.

Major improvements to existing static line performance could be achieved by either or both of two system modifications. The first is to utilize as large a radius as practical at the contact surface of the aircraft. This could be achieved by altering the aircraft door edge with a rounded channel of large bend diameter (radius). The second is to refit the existing static line inventory with sheathing in an effort to reduce the static line door edge interface friction. Either or both of these approaches would likely reflect the improvements in performance observed in the laboratory simulations.

INTENTIONALLY LEFT BLANK.

11. References

1. The Parachute Industry Association. "Webbing, Textiles, Woven Nylon." PIA-W-4088A, Skokie, IL, 1 March 1998.
2. Headquarters, Department of the Army. *Static Line Parachuting Techniques and Training*. FM 57-220, Washington, DC, 19 August 1996.
3. U.S. Federal Standard Test Method 191A. "Federal Standard for Textile Test Methods." Method 4108, 31 December 1968.
4. Millette, W., G. Thibault, R. Dooley, R. Kaste, and P. Mortaloni. "Investigation of Methods to Improve Static Line Effective Strength." Presented at the 16th Aerodynamic Decelerator Systems Seminar and Conference, Boston, MA, 21-24 May 2001.

INTENTIONALLY LEFT BLANK.

Appendix A. Bend Testing Fixture

Side View of Straight and Bend Fixture Gage Lengths

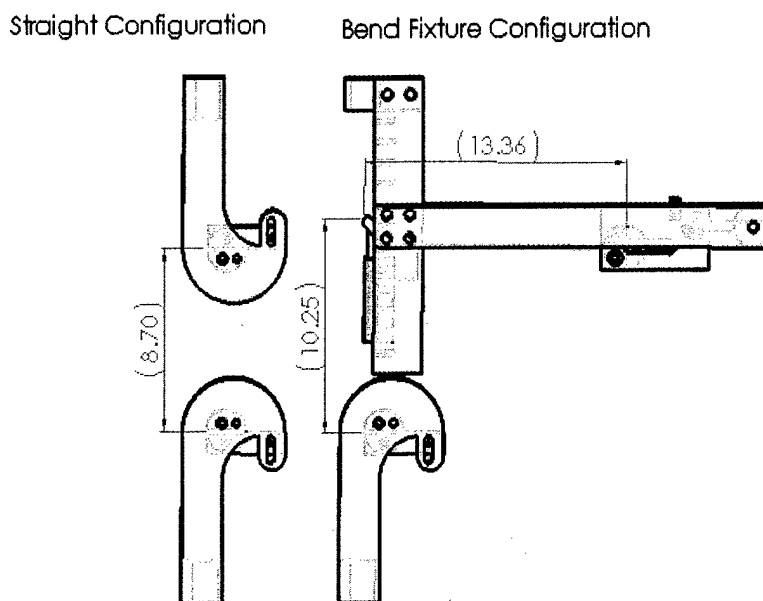


Figure A-1. Side view of straight and bend fixture gage lengths.

Table A-1. Table of minimum gage lengths.

Gage	Configuration	
	Straight (in)	90° Bend (in)
Vertical	8.7	10.3
Horizontal	0	13.4
Upper Grip Wrap (2 Wraps)	12.6	6.3 (one wrap upper grip)
Lower Grip Wrap (2 Wraps)	12.6	12.6
Total	33.9	42.6

Solid Model of Bend Fixture and Lower Grip

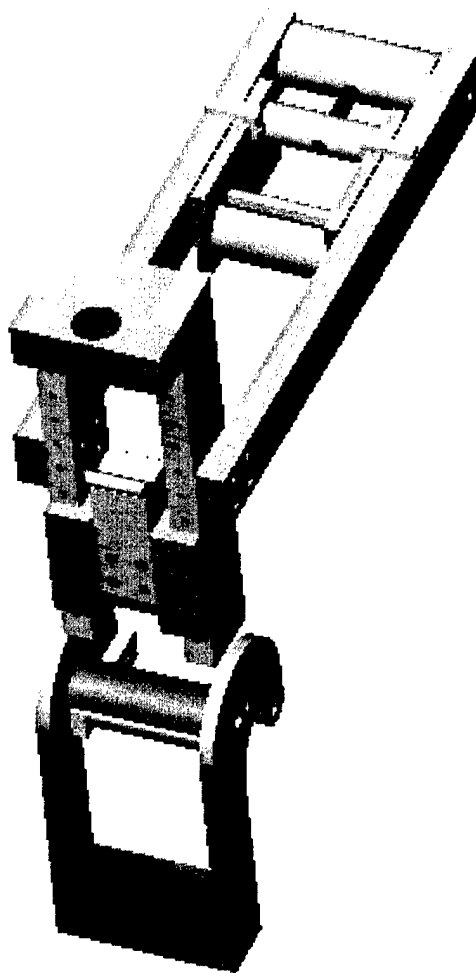


Figure A-2. Solid model of bend fixture and lower grip.

Pin Plate
(one per assembly)

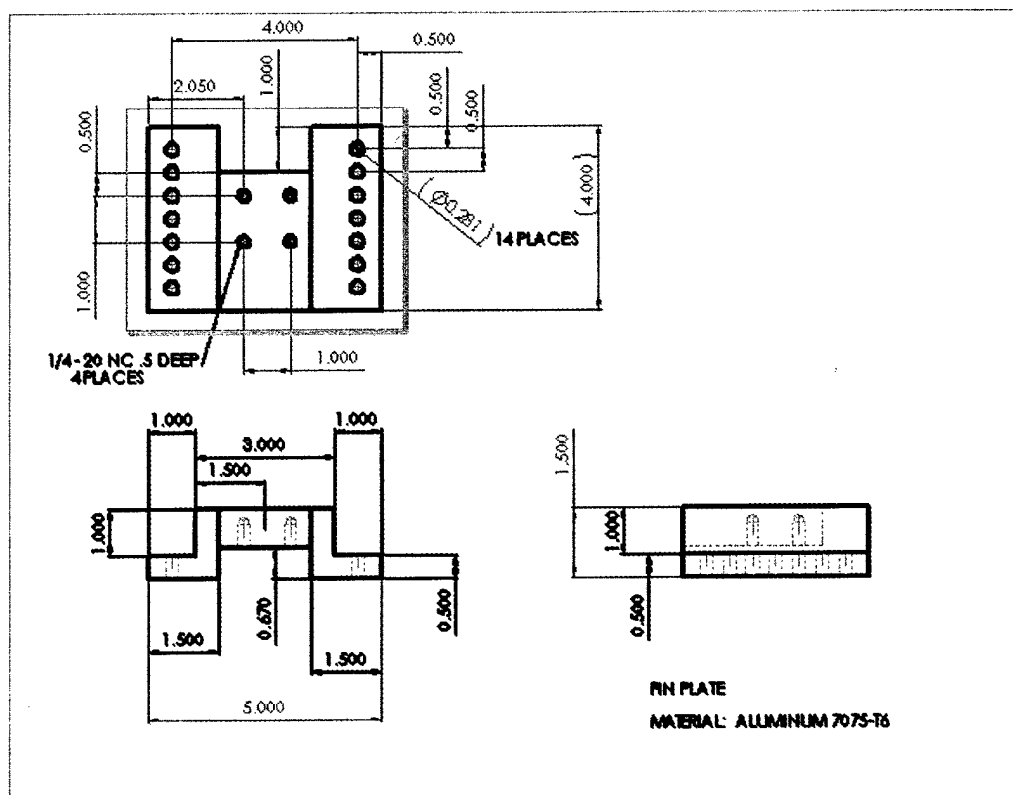


Figure A-3. Pin plate—aluminum.

Plate holder
(one per assembly)

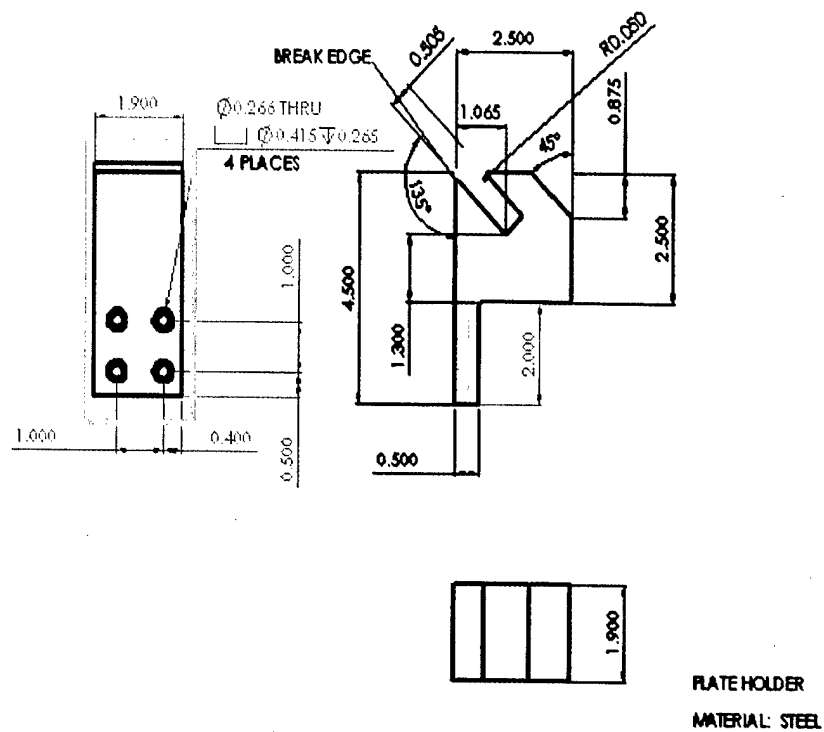


Figure A-4. Plate holder—steel.

Side Rail
(two per assembly)

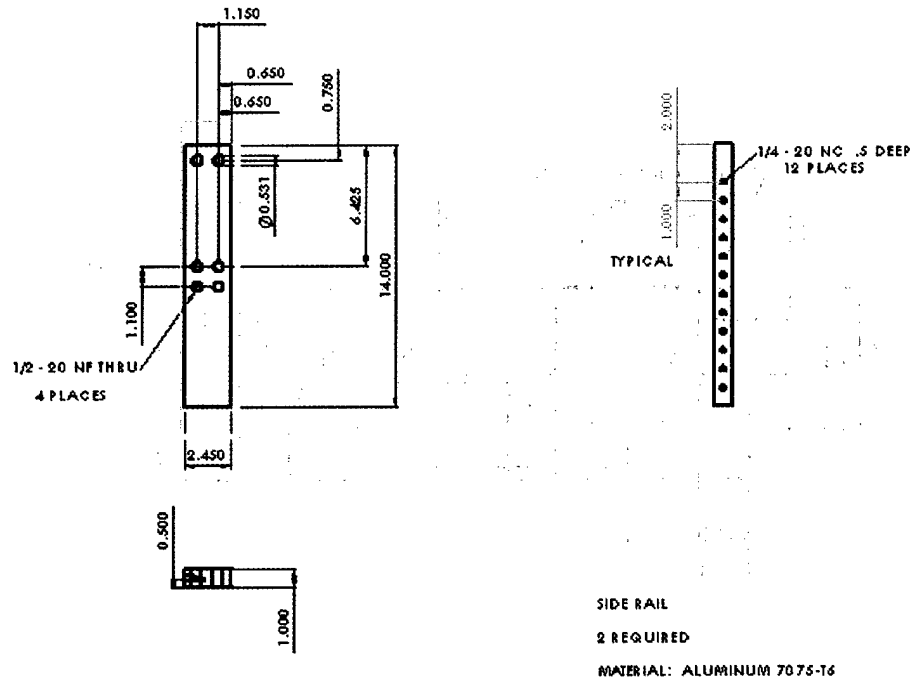


Figure A-5. Side rail—aluminum.

Top Plate
(one per assembly)

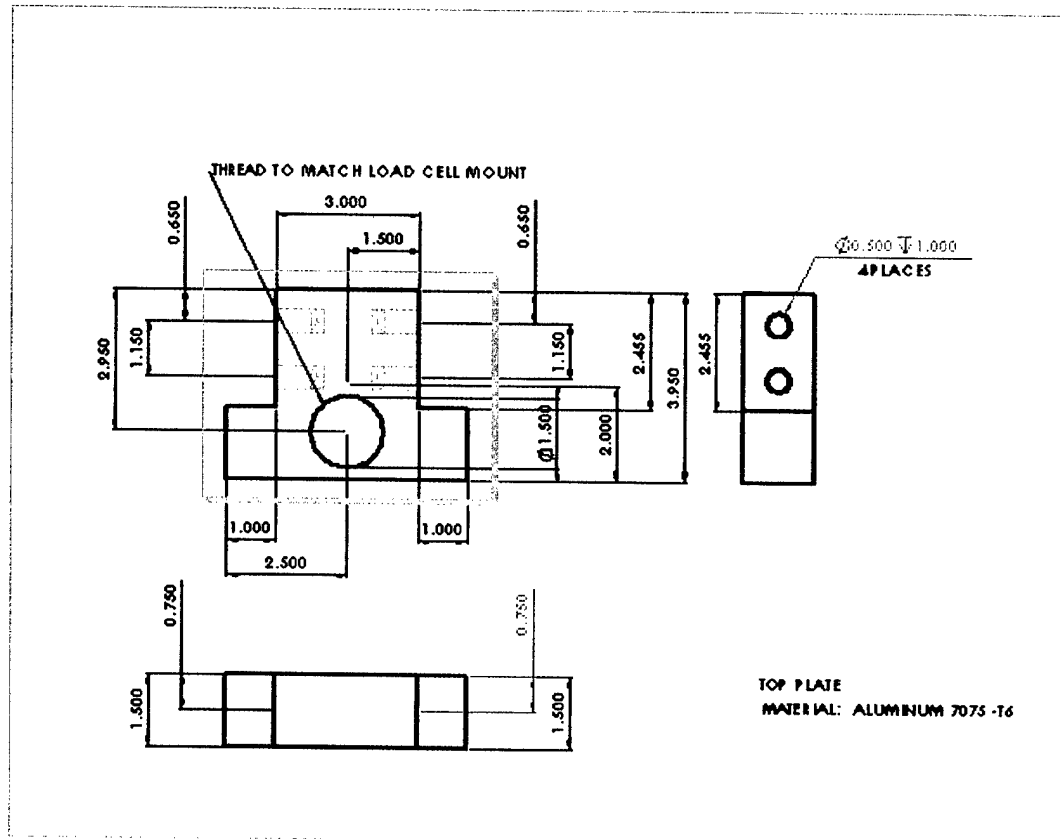


Figure A-6. Top plate—aluminum.

Trolley Anchor
(one per assembly)

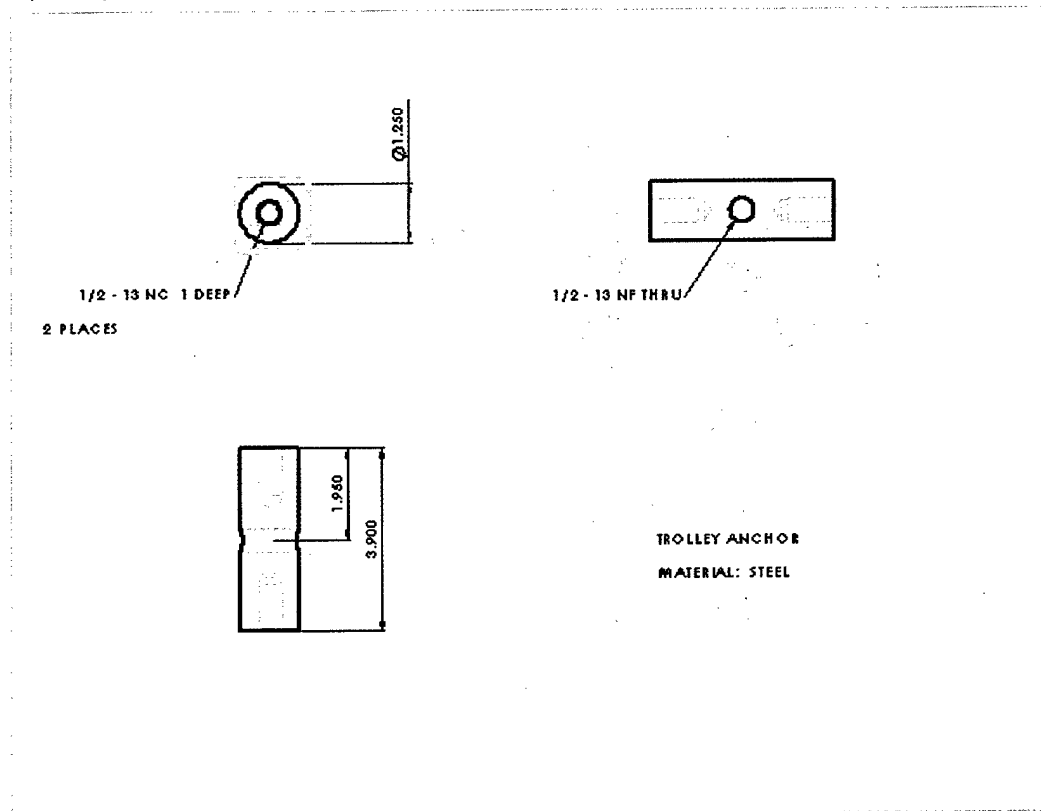


Figure A-7. Trolley anchor—steel.

Trolley Side Plate (Left)
(one per assembly)

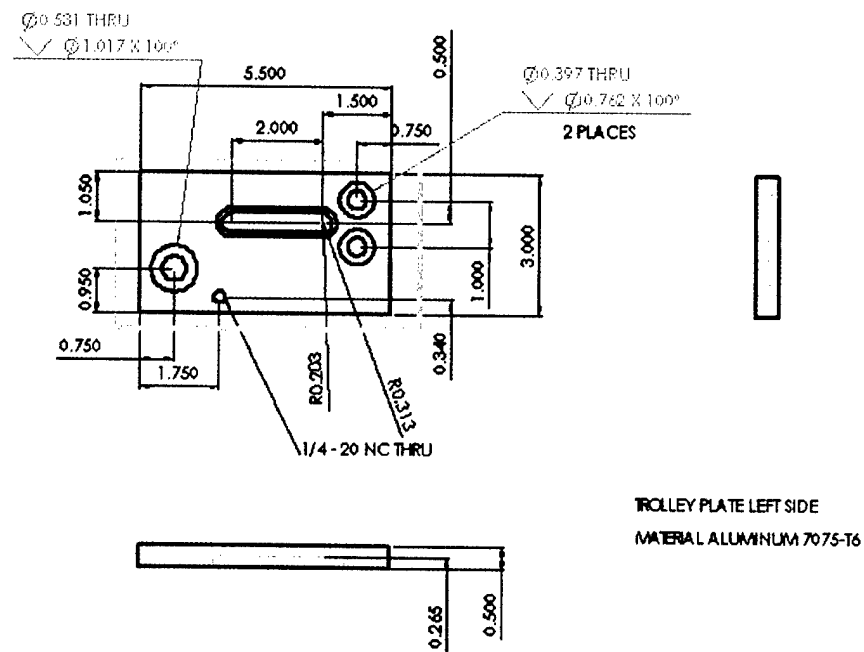


Figure A-8. Trolley side plate (left)—aluminum.

Trolley Side Plate (Right)
(one per assembly)

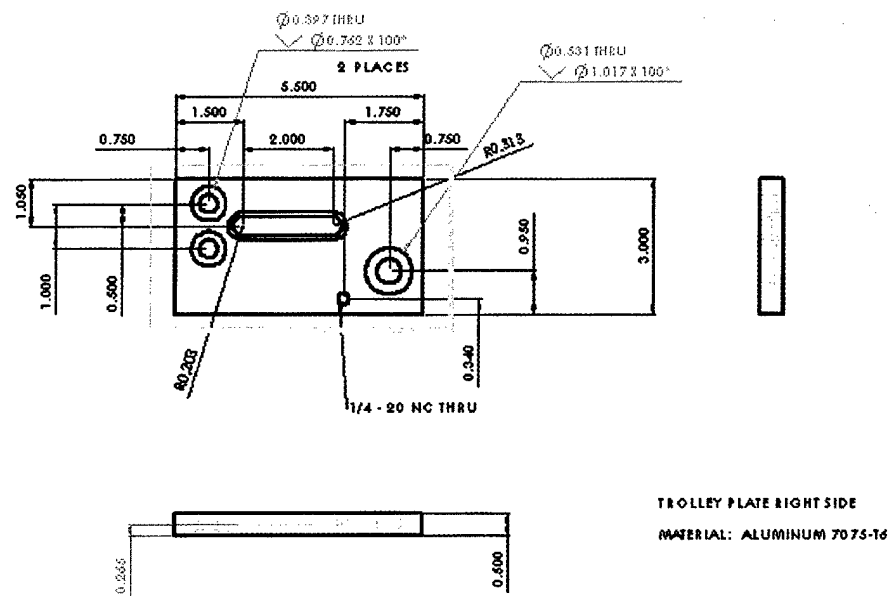


Figure A-9. Trolley side plate (right)—aluminum.

Trolley Stop
(two per assembly)

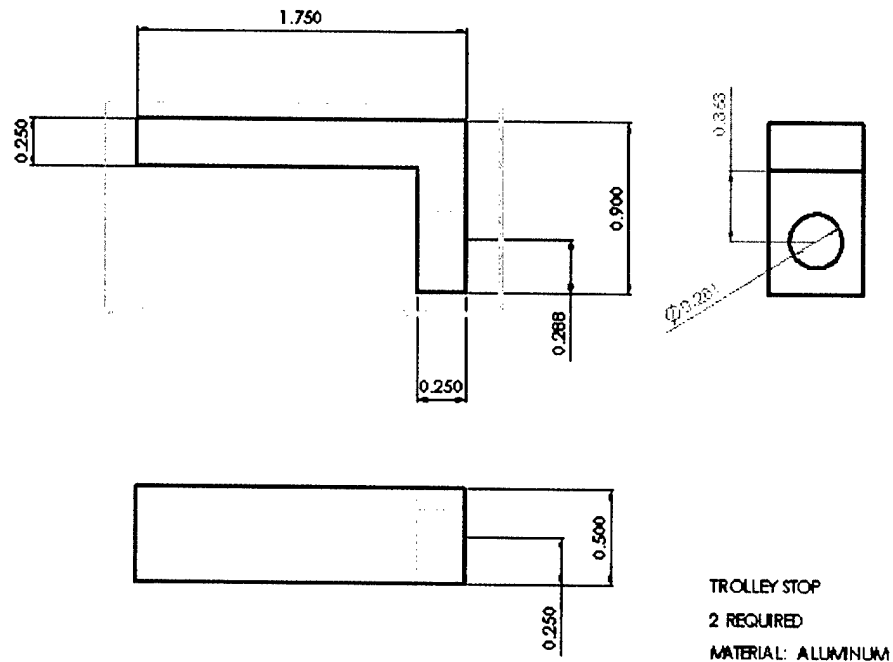


Figure A-10. Trolley stop—aluminum.

Trolley Rail (two per assembly)

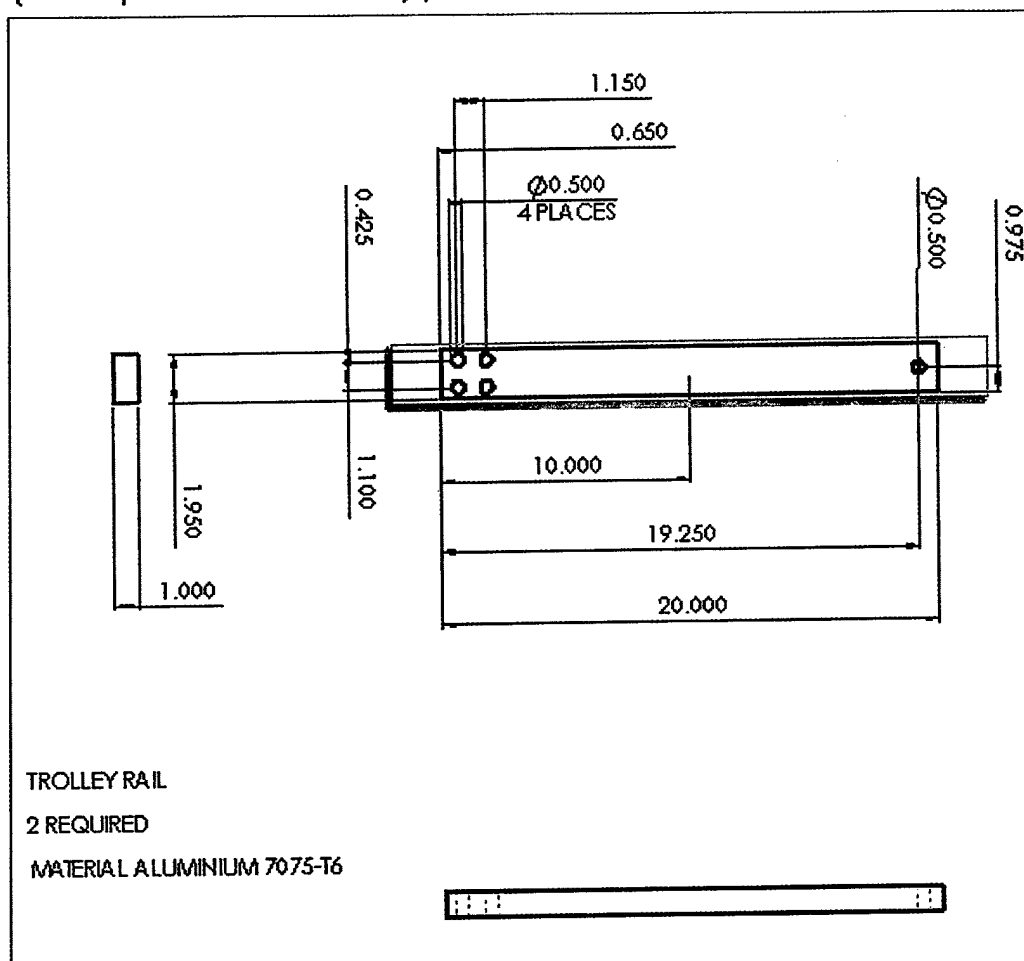
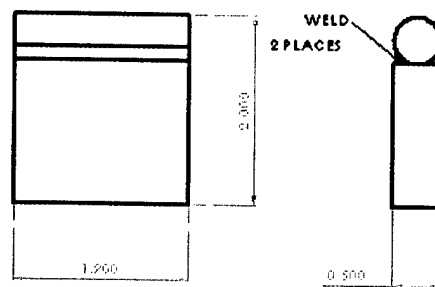


Figure A-11. Trolley rail—aluminum.

Typical Bend Plate
(0.500" rough shown)



ROUGH SURFACE BEND PLATE ASSEMBLY
MATERIALS: STEEL

Figure A-12. Typical bend plate—steel.

Appendix B. Typical Results Data

Sample load vs. displacement curves generated during tensile tests are shown in Figure B-1. This figure displays the individual load vs. displacement curves for the five specimens of test set 1 Type VIII (T-VIII), straight-pull configuration). Table B-1 shows the contents of the corresponding statistics report generated by the Instron Series IX software used to acquire test data and process results. Reports similar to Table B-1 were used to generate the tables in the main report.

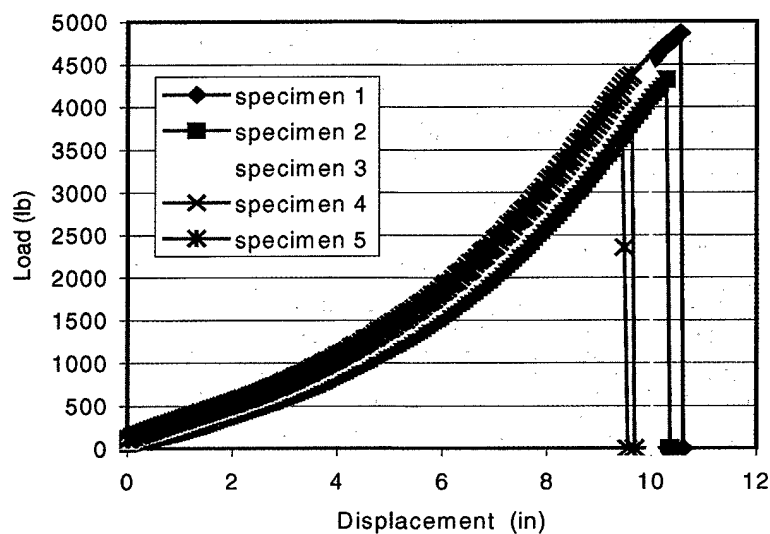


Figure B-1. Load vs. displacement curves for test set 1 of T-VIII webbing.

Table B-1. Statistics report for test set no. 1, T-VIII webbing.

Detail	Displacement at Maximum Load (in)	Load at Maximum Load (lbf)	Displacement at Auto Break (in)	Load at Auto Break (lbf)
Specimen no. 1	10.250	4346	10.250	4346
Specimen no. 2	10.550	4868	10.550	4868
Specimen no. 3	9.993	4443	9.933	4443
Specimen no. 4	9.440	4162	9.440	4162
Specimen no. 5	9.599	4374	9.599	4374
Mean	9.954	4439	9.954	4439
S.D.	0.456	262	0.456	262
C.V.	4.586	6	4.586	6
Median	9.933	4374	9.933	4374
Mean+2.00SD	10.867	4962	10.867	4962
Mean-2.00SD	9.041	3915	9.041	3915
Minimum	9.440	4162	9.440	4162
Maximum	10.550	4868	10.550	4868

Notes: S.D. = standard deviation; C.V. = coefficient of variation.

INTENTIONALLY LEFT BLANK.

NO. OF
COPIES ORGANIZATION

2 DEFENSE TECHNICAL
INFORMATION CENTER
DTIC OCA
8725 JOHN J KINGMAN RD
STE 0944
FT BELVOIR VA 22060-6218

1 HQDA
DAMO FDT
400 ARMY PENTAGON
WASHINGTON DC 20310-0460

1 OSD
OUSD(A&T)/ODDR&E(R)
DR R J TREW
3800 DEFENSE PENTAGON
WASHINGTON DC 20301-3800

1 COMMANDING GENERAL
US ARMY MATERIEL CMD
AMCRDA TF
5001 EISENHOWER AVE
ALEXANDRIA VA 22333-0001

1 INST FOR ADVNCD TCHNLGY
THE UNIV OF TEXAS AT AUSTIN
3925 W BRAKER LN STE 400
AUSTIN TX 78759-5316

1 US MILITARY ACADEMY
MATH SCI CTR EXCELLENCE
MADN MATH
THAYER HALL
WEST POINT NY 10996-1786

1 DIRECTOR
US ARMY RESEARCH LAB
AMSRL D
DR D SMITH
2800 POWDER MILL RD
ADELPHI MD 20783-1197

1 DIRECTOR
US ARMY RESEARCH LAB
AMSRL CI AI R
2800 POWDER MILL RD
ADELPHI MD 20783-1197

NO. OF
COPIES ORGANIZATION

3 DIRECTOR
US ARMY RESEARCH LAB
AMSRL CI LL
2800 POWDER MILL RD
ADELPHI MD 20783-1197

3 DIRECTOR
US ARMY RESEARCH LAB
AMSRL CI IS T
2800 POWDER MILL RD
ADELPHI MD 20783-1197

ABERDEEN PROVING GROUND

2 DIR USARL
AMSRL CI LP (BLDG 305)

<u>NO. OF COPIES</u>	<u>ORGANIZATION</u>
1	DIRECTOR US ARMY RESEARCH LAB AMSRL CP CA D SNIDER 2800 POWDER MILL RD ADELPHI MD 20783-1145
1	DIRECTOR US ARMY RESEARCH LAB AMSRL CI IS R 2800 POWDER MILL RD ADELPHI MD 20783-1145
3	DIRECTOR US ARMY RESEARCH LAB AMSRL OP SD TL 2800 POWDER MILL RD ADELPHI MD 20783-1145
1	DPTY ASST SECY FOR R&T SARD TT THE PENTAGON RM 3EA79 WASHINGTON DC 20301-7100
1	COMMANDER US ARMY MATERIEL CMD AMXMI INT 5001 EISENHOWER AVE ALEXANDRIA VA 22333-0001
4	COMMANDER US ARMY ARDEC AMSTA AR CC G PAYNE J GEHBAUER C BAULIEU H OPAT PICATINNY ARSENAL NJ 07806-5000
2	COMMANDER US ARMY ARDEC AMSTA AR AE WW E BAKER J PEARSON PICATINNY ARSENAL NJ 07806-5000

<u>NO. OF COPIES</u>	<u>ORGANIZATION</u>
1	COMMANDER US ARMY ARDEC AMSTA AR FSE PICATINNY ARSENAL NJ 07806-5000
1	COMMANDER US ARMY ARDEC AMSTA AR TD C SPINELLI PICATINNY ARSENAL NJ 07806-5000
6	COMMANDER US ARMY ARDEC AMSTA AR CCH A W ANDREWS S MUSALLI R CARR M LUCIANO E LOGSDEN T LOUZEIRO PICATINNY ARSENAL NJ 07806-5000
1	COMMANDER US ARMY ARDEC AMSTA AR CCH P J LUTZ PICATINNY ARSENAL NJ 07806-5000
1	COMMANDER US ARMY ARDEC AMSTA AR FSF T C LIVECCHIA PICATINNY ARSENAL NJ 07806-5000
1	COMMANDER US ARMY ARDEC AMSTA ASF PICATINNY ARSENAL NJ 07806-5000
1	COMMANDER US ARMY ARDEC AMSTA AR QAC T C C PATEL PICATINNY ARSENAL NJ 07806-5000

<u>NO. OF COPIES</u>	<u>ORGANIZATION</u>
1	COMMANDER US ARMY ARDEC AMSTA AR M D DEMELLA PICATINNY ARSENAL NJ 07806-5000
3	COMMANDER US ARMY ARDEC AMSTA AR FSA A WARNASH B MACHAK M CHIEFA PICATINNY ARSENAL NJ 07806-5000
2	COMMANDER US ARMY ARDEC AMSTA AR FSP G M SCHIKSNIS D CARLUCCI PICATINNY ARSENAL NJ 07806-5000
2	COMMANDER US ARMY ARDEC AMSTA AR CCH C H CHANIN S CHICO PICATINNY ARSENAL NJ 07806-5000
1	COMMANDER US ARMY ARDEC AMSTA AR QAC T D RIGOGLIOSO PICATINNY ARSENAL NJ 07806-5000
1	COMMANDER US ARMY ARDEC AMSTA AR WET T SACHAR BLDG 172 PICATINNY ARSENAL NJ 07806-5000

<u>NO. OF COPIES</u>	<u>ORGANIZATION</u>
1	US ARMY ARDEC INTELLIGENCE SPECIALIST AMSTA AR WEL F M GUERRIERE PICATINNY ARSENAL NJ 07806-5000
9	COMMANDER US ARMY ARDEC AMSTA AR CCH B P DONADIA F DONLON P VALENTI C KNUTSON G EUSTICE S PATEL G WAGNECZ R SAYER F CHANG PICATINNY ARSENAL NJ 07806-5000
6	COMMANDER US ARMY ARDEC AMSTA AR CCL F PUZYCKI R MCHUGH D CONWAY E JAROSZEWSKI R SCHLENNER M CLUNE PICATINNY ARSENAL NJ 07806-5000
1	PM ARMS SFAE GCSS ARMS BLDG 171 PICATINNY ARSENAL NJ 07806-5000
2	PEO FIELD ARTILLERY SYS SFAE FAS PM H GOLDMAN T MCWILLIAMS PICATINNY ARSENAL NJ 07806-5000

<u>NO. OF COPIES</u>	<u>ORGANIZATION</u>
1	COMMANDER US ARMY ARDEC AMSTA AR WEA J BRESCIA PICATINNY ARSENAL NJ 07806-5000
12	PM TMA SFAE GSSC TMA R MORRIS C KIMKER D GUZIEWICZ E KOPACZ R ROESER R DARCY R KOWALSKI R MCDANOLDS L D ULISSE C ROLLER J MCGREEN B PATER PICATINNY ARSENAL NJ 07806-5000
1	COMMANDER US ARMY ARDEC PRODUCTION BASE MODERN ACTY AMSMC PBM K PICATINNY ARSENAL NJ 07806-5000
1	COMMANDER US ARMY TACOM PM ABRAMS SFAE ASM AB 6501 ELEVEN MILE RD WARREN MI 48397-5000
1	COMMANDER US ARMY TACOM AMSTA SF WARREN MI 48397-5000
1	COMMANDER US ARMY TACOM PM BFVS SFAE GCSS W BV 6501 ELEVEN MILE RD WARREN MI 48397-5000

<u>NO. OF COPIES</u>	<u>ORGANIZATION</u>
1	DIRECTOR AIR FORCE RESEARCH LAB MLLMD D MIRACLE 2230 TENTH ST WRIGHT PATTERSON AFB OH 45433-7817
1	OFC OF NAVAL RESEARCH J CHRISTODOULOU ONR CODE 332 800 N QUINCY ST ARLINGTON VA 22217-5600
1	US ARMY CERL R LAMPO 2902 NEWMARK DR CHAMPAIGN IL 61822
1	COMMANDER US ARMY TACOM PM SURVIVABLE SYSTEMS SFAE GCSS W GSI H M RYZYI 6501 ELEVEN MILE RD WARREN MI 48397-5000
1	COMMANDER US ARMY TACOM CHIEF ABRAMS TESTING SFAE GCSS W AB QT T KRASKIEWICZ 6501 ELEVEN MILE RD WARREN MI 48397-5000
1	COMMANDER WATERVLIET ARSENAL SMCWV QAE Q B VANINA BLDG 44 WATERVLIET NY 12189-4050
3	ARMOR SCHOOL ATZK TD R BAUEN J BERG A POMEY FT KNOX KY 40121

NO. OF
COPIES ORGANIZATION

2 HQ IOC TANK
AMMUNITION TEAM
AMSIO SMT
R CRAWFORD
W HARRIS
ROCK ISLAND IL 61299-6000

2 COMMANDER
US ARMY AMCOM
AVIATION APPLIED TECH DIR
J SCHUCK
FT EUSTIS VA 23604-5577

14 COMMANDER
US ARMY TACOM
AMSTA TR R
R MCCLELLAND
D THOMAS
J BENNETT
D HANSEN
AMSTA JSK
S GOODMAN
J FLORENCE
K IYER
D TEMPLETON
A SCHUMACHER
AMSTA TR D
D OSTBERG
L HINOJOSA
B RAJU
AMSTA CS SF
H HUTCHINSON
F SCHWARZ
WARREN MI 48397-5000

14 BENET LABORATORIES
AMSTA AR CCB
R FISCELLA
M SOJA
E KATHE
M SCAVULO
G SPENCER
P WHEELER
S KRUPSKI
J VASILAKIS
G FRIAR
R HASENBEIN
AMSTA CCB R
S SOPOK
E HYLAND
D CRAYON
R DILLON
WATERVLIET NY 12189-4050

NO. OF
COPIES ORGANIZATION

1 DIRECTOR
US ARMY AMCOM
SFAE AV RAM TV
D CALDWELL
BLDG 5300
REDSTONE ARSENAL AL
35898

1 NAVAL SURFACE WARFARE CTR
DAHLGREN DIV CODE G06
DAHLGREN VA 22448

2 US ARMY CORPS OF ENGINEERS
CERD C
T LIU
CEW ET
T TAN
20 MASS AVE NW
WASHINGTON DC 20314

1 US ARMY COLD REGIONS
RSCH & ENGRNG LAB
P DUTTA
72 LYME RD
HANOVER NH 03755

1 USA SBCCOM PM SOLDIER SPT
AMSSB PM RSS A
J CONNORS
KANSAS ST
NATICK MA 01760-5057

2 USA SBCCOM
MATERIAL SCIENCE TEAM
AMSSB RSS
J HERBERT
M SENNETT
KANSAS ST
NATICK MA 01760-5057

2 OFC OF NAVAL RESEARCH
D SIEGEL CODE 351
J KELLY
800 N QUINCY ST
ARLINGTON VA 22217-5660

1 NAVAL SURFACE WARFARE CTR
TECH LIBRARY CODE 323
17320 DAHLGREN RD
DAHLGREN VA 22448

<u>NO. OF COPIES</u>	<u>ORGANIZATION</u>	<u>NO. OF COPIES</u>	<u>ORGANIZATION</u>
1	NAVAL SURFACE WARFARE CTR CRANE DIVISION M JOHNSON CODE 20H4 LOUISVILLE KY 40214-5245	8	US ARMY SBCCOM SOLDIER SYSTEMS CENTER BALLISTICS TEAM J WARD W ZUKAS P CUNNIFF J SONG MARINE CORPS TEAM J MACKIEWICZ BUS AREA ADVOCACY TEAM W HASKELL AMSSB RCP SS W NYKVIST S BEAUDOIN KANSAS ST NATICK MA 01760-5019
2	NAVAL SURFACE WARFARE CTR U SORATHIA C WILLIAMS CD 6551 9500 MACARTHUR BLVD WEST BETHESDA MD 20817		
2	COMMANDER NAVAL SURFACE WARFARE CTR CARDEROCK DIVISION R PETERSON CODE 2020 M CRITCHFIELD CODE 1730 BETHESDA MD 20084		
8	DIRECTOR US ARMY NATIONAL GROUND INTELLIGENCE CTR D LEITER MS 404 M HOLTUS MS 301 M WOLFE MS 307 S MINGLEDORF MS 504 J GASTON MS 301 W GSTATTENBAUER MS 304 R WARNER MS 305 J CRIDER MS 306 220 SEVENTH ST NE CHARLOTTESVILLE VA 22091	7	US ARMY RESEARCH OFC A CROWSON H EVERETT J PRATER G ANDERSON D STEPP D KISEROW J CHANG PO BOX 12211 RESEARCH TRIANGLE PARK NC 27709-2211
1	NAVAL SEA SYSTEMS CMD D LIESE 2531 JEFFERSON DAVIS HWY ARLINGTON VA 22242-5160	8	NAVAL SURFACE WARFARE CTR J FRANCIS CODE G30 D WILSON CODE G32 R D COOPER CODE G32 J FRAYSSE CODE G33 E ROWE CODE G33 T DURAN CODE G33 L DE SIMONE CODE G33 R HUBBARD CODE G33 DAHLGREN VA 22448
1	NAVAL SURFACE WARFARE CTR M LACY CODE B02 17320 DAHLGREN RD DAHLGREN VA 22448	2	NAVAL SURFACE WARFARE CTR CARDEROCK DIVISION R CRANE CODE 2802 C WILLIAMS CODE 6553 3A LEGGETT CIR BETHESDA MD 20054-5000
1	EXPEDITIONARY WARFARE DIV N85 F SHOUP 2000 NAVY PENTAGON WASHINGTON DC 20350-2000	1	AFRL MLBC 2941 P ST RM 136 WRIGHT PATTERSON AFB OH 45433-7750

NO. OF
COPIES ORGANIZATION

1 AFRL MLSS
R THOMSON
2179 12TH ST RM 122
WRIGHT PATTERSON AFB OH
45433-7718

2 AFRL
F ABRAMS
J BROWN
BLDG 653
2977 P ST STE 6
WRIGHT PATTERSON AFB OH
45433-7739

1 WATERWAYS EXPERIMENT
D SCOTT
3909 HALLS FERRY RD SC C
VICKSBURG MS 39180

5 DIRECTOR
LLNL
R CHRISTENSEN
S DETERESA
F MAGNESS
M FINGER MS 313
M MURPHY L 282
PO BOX 808
LIVERMORE CA 94550

1 AFRL MLS OL
L COULTER
5851 F AVE
BLDG 849 RM AD1A
HILL AFB UT 84056-5713

1 OSD
JOINT CCD TEST FORCE
OSD JCCD
R WILLIAMS
3909 HALLS FERRY RD
VICKSBURG MS 29180-6199

3 DARPA
M VANFOSSSEN
S WAX
L CHRISTODOULOU
3701 N FAIRFAX DR
ARLINGTON VA 22203-1714

1 DIRECTOR
LOS ALAMOS NATIONAL LAB
F L ADDESSIO T 3 MS 5000
PO BOX 1633
LOS ALAMOS NM 87545

NO. OF
COPIES ORGANIZATION

2 SERDP PROGRAM OFC
PM P2
C PELLERIN
B SMITH
901 N STUART ST STE 303
ARLINGTON VA 22203

1 US DEPT OF ENERGY
OFC OF ENVIRONMENTAL
MANAGEMENT
P RITZCOVAN
19901 GERMANTOWN RD
GERMANTOWN MD 20874-1928

1 OAK RIDGE NATIONAL
LABORATORY
R M DAVIS
PO BOX 2008
OAK RIDGE TN 37831-6195

1 OAK RIDGE NATIONAL
LABORATORY
C EBERLE MS 8048
PO BOX 2008
OAK RIDGE TN 37831

3 DIRECTOR
SANDIA NATIONAL LABS
APPLIED MECHANICS DEPT
MS 9042
J HANDROCK
Y R KAN
J LAUFFER
PO BOX 969
LIVERMORE CA 94551-0969

1 OAK RIDGE NATIONAL
LABORATORY
C D WARREN MS 8039
PO BOX 2008
OAK RIDGE TN 37831

4 NIST
M VANLANDINGHAM MS 8621
J CHIN MS 8621
J MARTIN MS 8621
D DUTHINH MS 8611
100 BUREAU DR
GAITHERSBURG MD 20899

<u>NO. OF COPIES</u>	<u>ORGANIZATION</u>
1	HYDROGEOLOGIC INC SERDP ESTCP SPT OFC S WALSH 1155 HERNDON PKWY STE 900 HERNDON VA 20170
3	NASA LANGLEY RSCH CTR AMSRL VS W ELBER MS 266 F BARTLETT JR MS 266 G FARLEY MS 266 HAMPTON VA 23681-0001
1	NASA LANGLEY RSCH CTR T GATES MS 188E HAMPTON VA 23661-3400
1	FHWA E MUNLEY 6300 GEORGETOWN PIKE MCLEAN VA 22101
1	USDOT FEDERAL RAILRD M FATEH RDV 31 WASHINGTON DC 20590
3	CYTEC FIBERITE R DUNNE D KOHLI R MAYHEW 1300 REVOLUTION ST HAVRE DE GRACE MD 21078
1	MARINE CORPS INTLLGNC ACTVTY D KOSITZKE 3300 RUSSELL RD STE 250 QUANTICO VA 22134-5011
1	DIRECTOR NATIONAL GRND INTLLGNC CTR IANG TMT 220 SEVENTH ST NE CHARLOTTESVILLE VA 22902-5396
1	SIOUX MFG B KRIEL PO BOX 400 FT TOTTEN ND 58335

<u>NO. OF COPIES</u>	<u>ORGANIZATION</u>
2	3TEX CORPORATION A BOGDANOVICH J SINGLETARY 109 MACKENAN DR CARY NC 27511
1	3M CORPORATION J SKILDUM 3M CENTER BLDG 60 IN 01 ST PAUL MN 55144-1000
1	DIRECTOR DEFENSE INTLLGNC AGNCY TA 5 K CRELLING WASHINGTON DC 20310
1	ADVANCED GLASS FIBER YARNS T COLLINS 281 SPRING RUN LANE STE A DOWNINGTON PA 19335
1	COMPOSITE MATERIALS INC D SHORTT 19105 63 AVE NE PO BOX 25 ARLINGTON WA 98223
1	JPS GLASS L CARTER PO BOX 260 SLATER RD SLATER SC 29683
1	COMPOSITE MATERIALS INC R HOLLAND 11 JEWEL CT ORINDA CA 94563
1	COMPOSITE MATERIALS INC C RILEY 14530 S ANSON AVE SANTA FE SPRINGS CA 90670
2	SIMULA J COLTMAN R HUYETT 10016 S 51ST ST PHOENIX AZ 85044

<u>NO. OF COPIES</u>	<u>ORGANIZATION</u>	<u>NO. OF COPIES</u>	<u>ORGANIZATION</u>
2	PROTECTION MATERIALS INC M MILLER F CRILLEY 14000 NW 58 CT MIAMI LAKES FL 33014	1	NATIONAL COMPOSITE CENTER T CORDELL 2000 COMPOSITE DR KETTERING OH 45420
2	FOSTER MILLER M ROYLANCE W ZUKAS 195 BEAR HILL RD WALTHAM MA 02354-1196	3	PACIFIC NORTHWEST LAB M SMITH G VAN ARSDALE R SHIPPELL PO BOX 999 RICHLAND WA 99352
1	ROM DEVELOPMENT CORP R O MEARA 136 SWINEBURNE ROW BRICK MARKET PLACE NEWPORT RI 02840	2	AMOCO PERFORMANCE PRODUCTS M MICHNO JR J BANISAUKAS 4500 MCGINNIS FERRY RD ALPHARETTA GA 30202-3944
2	TEXTRON SYSTEMS T FOLTZ M TREASURE 1449 MIDDLESEX ST LOWELL MA 01851	8	ALLIANT TECHSYSTEMS INC C CANDLAND MN11 2830 C AAKHUS MN11 2830 B SEE MN11 2439 N VLAHAKUS MN11 2145 R DOHRN MN11 2830 S HAGLUND MN11 2439 M HISSONG MN11 2830 D KAMDAR MN11 2830 600 SECOND ST NE HOPKINS MN 55343-8367
1	O GARA HESS & EISENHARDT M GILLESPIE 9113 LESAINTE DR FAIRFIELD OH 45014	1	SAIC M PALMER 1410 SPRING HILL RD STE 400 MS SH4 5 MCLEAN VA 22102
2	MILLIKEN RSCH CORP H KUHN M MACLEOD PO BOX 1926 SPARTANBURG SC 29303	1	APPLIED COMPOSITES W GRISCH 333 NORTH SIXTH ST ST CHARLES IL 60174
1	CONNEAUGHT INDUSTRIES INC J SANTOS PO BOX 1425 COVENTRY RI 02816	1	CUSTOM ANALYTICAL ENG SYS INC A ALEXANDER 13000 TENSOR LANE NE FLINTSTONE MD 21530
1	BATTELLE NATICK OPNS B HALPIN 209 W CENTRAL ST STE 302 NATICK MA 01760		
1	ARMTEC DEFENSE PRODUCTS S DYER 85 901 AVE 53 PO BOX 848 COACHELLA CA 92236		

<u>NO. OF COPIES</u>	<u>ORGANIZATION</u>
1	OFC DEPUTY UNDER SEC DEFNS J THOMPSON 1745 JEFFERSON DAVIS HWY CRYSTAL SQ 4 STE 501 ARLINGTON VA 22202
3	ALLIANT TECHSYSTEMS INC J CONDON E LYNAM J GERHARD WV01 16 STATE RT 956 PO BOX 210 ROCKET CENTER WV 26726-0210
1	PROJECTILE TECHNOLOGY INC 515 GILES ST HAVRE DE GRACE MD 21078
1	HEXCEL INC R BOE PO BOX 18748 SALT LAKE CITY UT 84118
5	AEROJET GEN CORP D PILLASCH T COULTER C FLYNN D RUBAREZUL M GREINER 1100 WEST HOLLYVALE ST AZUSA CA 91702-0296
1	HERCULES INC HERCULES PLAZA WILMINGTON DE 19894
1	BRIGS COMPANY J BACKOFEN 2668 PETERBOROUGH ST HERNDON VA 22071-2443
1	ZERNOW TECHNICAL SERVICES L ZERNOW 425 W BONITA AVE STE 208 SAN DIMAS CA 91773
1	GENERAL DYNAMICS OTS L WHITMORE 10101 NINTH ST NORTH ST PETERSBURG FL 33702

<u>NO. OF COPIES</u>	<u>ORGANIZATION</u>
3	GENERAL DYNAMICS OTS FLINCHBAUGH DIV E STEINER B STEWART T LYNCH PO BOX 127 RED LION PA 17356
1	GKN AEROSPACE D OLDS 15 STERLING DR WALLINGFORD CT 06492
5	SIKORSKY AIRCRAFT G JACARUSO T CARSTENSAN B KAY S GARBO MS S330A J ADELMANN 6900 MAIN ST PO BOX 9729 STRATFORD CT 06497-9729
1	PRATT & WHITNEY C WATSON 400 MAIN ST MS 114 37 EAST HARTFORD CT 06108
1	AEROSPACE CORP G HAWKINS M4 945 2350 E EL SEGUNDO BLVD EL SEGUNDO CA 90245
2	CYTEC FIBERITE M LIN W WEB 1440 N KRAEMER BLVD ANAHEIM CA 92806
1	UDLP G THOMAS PO BOX 58123 SANTA CLARA CA 95052
2	UDLP R BARRETT MAIL DROP M53 V HORVATICH MAIL DROP M53 328 W BROKAW RD SANTA CLARA CA 95052-0359

<u>NO. OF COPIES</u>	<u>ORGANIZATION</u>
3	UDLP GROUND SYSTEMS DIVISION M PEDRAZZI MAIL DROP N09 A LEE MAIL DROP N11 M MACLEAN MAIL DROP N06 1205 COLEMAN AVE SANTA CLARA CA 95052
2	UDLP R BRYNSVOLD P JANKE MS 170 4800 EAST RIVER RD MINNEAPOLIS MN 55421-1498
2	BOEING ROTORCRAFT P MINGURT P HANDEL 800 B PUTNAM BLVD WALLINGFORD PA 19086
1	BOEING DOUGLAS PRODUCTS DIV L J HART SMITH 3855 LAKEWOOD BLVD D800 0019 LONG BEACH CA 90846-0001
1	LOCKHEED MARTIN SKUNK WORKS D FORTNEY 1011 LOCKHEED WAY PALMDALE CA 93599-2502
1	LOCKHEED MARTIN R FIELDS 1195 IRWIN CT WINTER SPRINGS FL 32708
1	MATERIALS SCIENCES CORP G FLANAGAN 500 OFC CENTER DR STE 250 FT WASHINGTON PA 19034
1	NORTHROP GRUMMAN CORP ELECTRONIC SENSORS & SYSTEMS DIV E SCHOCH MS V 16 1745A W NURSERY RD LINTHICUM MD 21090

<u>NO. OF COPIES</u>	<u>ORGANIZATION</u>
1	GDLS DIVISION D BARTLE PO BOX 1901 WARREN MI 48090
2	GDLS D REES M PASIK PO BOX 2074 WARREN MI 48090-2074
1	GDLS MUSKEGON OPERATIONS W SOMMERS JR 76 GETTY ST MUSKEGON MI 49442
1	GENERAL DYNAMICS AMPHIBIOUS SYS SURVIVABILITY LEAD G WALKER 991 ANNAPOLIS WAY WOODBIDGE VA 22191
6	INST FOR ADVANCED TECH H FAIR I MCNAB P SULLIVAN S BLESS W REINECKE C PERSAD 3925 W BRAKER LN STE 400 AUSTIN TX 78759-5316
2	CIVIL ENGR RSCH FOUNDATION PRESIDENT H BERNSTEIN R BELLE 1015 15TH ST NW STE 600 WASHINGTON DC 20005
1	ARROW TECH ASSO 1233 SHELBURNE RD STE D8 SOUTH BURLINGTON VT 05403-7700
1	R EICHELBERGER CONSULTANT 409 W CATHERINE ST BEL AIR MD 21014-3613

<u>NO. OF COPIES</u>	<u>ORGANIZATION</u>
1	UCLA MANE DEPT ENGR IV H T HAHN LOS ANGELES CA 90024-1597
2	UNIV OF DAYTON RESEARCH INST R Y KIM A K ROY 300 COLLEGE PARK AVE DAYTON OH 45469-0168
1	UMASS LOWELL PLASTICS DEPT N SCHOTT 1 UNIVERSITY AVE LOWELL MA 01854
1	IIT RESEARCH CENTER D ROSE 201 MILL ST ROME NY 13440-6916
1	GA TECH RSCH INST GA INST OF TCHNLGY P FRIEDERICH ATLANTA GA 30392
1	MICHIGAN ST UNIV MSM DEPT R AVERILL 3515 EB EAST LANSING MI 48824-1226
1	UNIV OF WYOMING D ADAMS PO BOX 3295 LARAMIE WY 82071
2	PENN STATE UNIV R MCNITT C BAKIS 212 EARTH ENGR SCIENCES BLDG UNIVERSITY PARK PA 16802
1	PENN STATE UNIV R S ENGEL 245 HAMMOND BLDG UNIVERSITY PARK PA 16801

<u>NO. OF COPIES</u>	<u>ORGANIZATION</u>
1	PURDUE UNIV SCHOOL OF AERO & ASTRO C T SUN W LAFAYETTE IN 47907-1282
1	STANFORD UNIV DEPT OF AERONAUTICS & AEROBALLISTICS S TSAI DURANT BLDG STANFORD CA 94305
1	UNIV OF MAINE ADV STR & COMP LAB R LOPEZ ANIDO 5793 AEWB BLDG ORONO ME 04469-5793
1	JOHNS HOPKINS UNIV APPLIED PHYSICS LAB P WIENHOLD 11100 JOHNS HOPKINS RD LAUREL MD 20723-6099
1	UNIV OF DAYTON J M WHITNEY COLLEGE PARK AVE DAYTON OH 45469-0240
5	UNIV OF DELAWARE CTR FOR COMPOSITE MTRLs J GILLESPIE M SANTARE S YARLAGADDA S ADVANI D HEIDER 201 SPENCER LABORATORY NEWARK DE 19716
1	DEPT OF MATERIALS SCIENCE & ENGINEERING UNIVERSITY OF ILLINOIS AT URBANA CHAMPAIGN J ECONOMY 1304 WEST GREEN ST 115B URBANA IL 61801
1	NORTH CAROLINA STATE UNIV CIVIL ENGINEERING DEPT W RASDORF PO BOX 7908 RALEIGH NC 27696-7908

NO. OF
COPIES ORGANIZATION

1 UNIV OF MARYLAND
DEPT OF AEROSPACE ENGNRNG
A J VIZZINI
COLLEGE PARK MD 20742

1 DREXEL UNIV
A S D WANG
32ND & CHESTNUT ST
PHILADELPHIA PA 19104

3 UNIV OF TEXAS AT AUSTIN
CTR FOR ELECTROMECHANICS
J PRICE
A WALLS
J KITZMILLER
10100 BURNET RD
AUSTIN TX 78758-4497

3 VA POLYTECHNICAL
INST & STATE UNIV
DEPT OF ESM
M W HYER
K REIFSNIDER
R JONES
BLACKSBURG VA 24061-0219

1 SOUTHWEST RSCH INST
ENGR & MATL SCIENCES DIV
J RIEGEL
6220 CULEBRA RD
PO DRAWER 28510
SAN ANTONIO TX 78228-0510

ABERDEEN PROVING GROUND

1 US ARMY MATERIEL
SYSTEMS ANALYSIS ACTIVITY
P DIETZ
392 HOPKINS RD
AMXS TD
APG MD 21005-5071

1 DIRECTOR
US ARMY RESEARCH LAB
AMSRL OP AP L
APG MD 21005-5066

90 DIR USARL
AMSRL CI
AMSRL CI S
A MARK

NO. OF
COPIES ORGANIZATION

ABERDEEN PROVING GROUND (CONT)

AMSRL CS IO FI
M ADAMSON

AMSRL SL BA
AMSRL SL BL
D BELY
R HENRY

AMSRL SL BG
AMSRL SL I
AMSRL WM

J SMITH
AMSRL WM B
A HORST

AMSRL WM BA
D LYON

AMSRL WM BC
P PLOSTINS

J NEWILL
S WILKERSON
A ZIELINSKI

AMSRL WM BD
B FORCH
R FIFER

R PESCE RODRIGUEZ
B RICE

AMSRL WM BE
C LEVERITT

AMSRL WM BF
J LACETERA

AMSRL WM BR
C SHOEMAKER

J BORNSTEIN
AMSRL WM M

D VIECHNICKI
G HAGNAUER

J MCCAULEY
AMSRL WM MA

L GHIORSE
S MCKNIGHT

AMSRL WM MB
B FINK

J BENDER
T BOGETTI

R BOSSOLI
L BURTON

K BOYD
S CORNELISON

P DEHMER
R DOOLEY

W DRYSDALE
G GAZONAS

NO. OF
COPIES ORGANIZATION

ABERDEEN PROVING GROUND (CONT)

S GHIORSE
D GRANVILLE
D HOPKINS
C HOPPEL
D HENRY
R KASTE
M KLUSEWITZ
M LEADORE
R LIEB
E RIGAS
J SANDS
D SPAGNUOLO
W SPURGEON
J TZENG
E WETZEL
A FRYDMAN
AMRSL WM MC
J BEATTY
E CHIN
J MONTGOMERY
A WERECZCAK
J LASALVIA
J WELLS
AMRSL WM MD
W ROY
S WALSH
AMRSL WM T
B BURNS
M ZOLTOSKI
AMRSL WM TA
W GILLICH
T HAVEL
J RUNYEON
M BURKINS
E HORWATH
B GOOCH
W BRUCHEY
M NORMANDIA
AMRSL WM TB
D KOOKER
P BAKER
AMRSL WM TC
R COATES

NO. OF
COPIES ORGANIZATION

ABERDEEN PROVING GROUND (CONT)

AMRSL WM TD
A DAS GUPTA
T HADUCH
T MOYNIHAN
F GREGORY
M RAFTENBERG
M BOTELER
T WEERASOORIYA
D DANDEKAR
A DIETRICH
AMRSL WM TE
A NIILER
J POWELL
AMRSL SS SD
H WALLACE
AMRSL SS SE DS
R REYZER
R ATKINSON

NO. OF
COPIES ORGANIZATION

1 LTD
R MARTIN
MERL
TAMWORTH RD
HERTFORD SG13 7DG
UK

1 SMC SCOTLAND
P W LAY
DERA ROSYTH
ROSYTH ROYAL DOCKYARD
DUNFERMLINE FIFE KY 11 2XR
UK

1 CIVIL AVIATION
ADMINISTRATION
T GOTTESMAN
PO BOX 8
BEN GURION INTERNL AIRPORT
LOD 70150
ISRAEL

1 AEROSPATIALE
S ANDRE
A BTE CC RTE MD132
316 ROUTE DE BAYONNE
TOULOUSE 31060
FRANCE

1 DRA FORT HALSTEAD
P N JONES
SEVEN OAKS KENT TN 147BP
UK

1 DEFENSE RESEARCH ESTAB
VALCARTIER
F LESAGE
COURCELETTE QUEBEC
COA IRO
CANADA

1 SWISS FEDERAL ARMAMENTS
WKS
W LANZ
ALLMENDSTRASSE 86
3602 THUN
SWITZERLAND

NO. OF
COPIES ORGANIZATION

1 DYNAMEC RESEARCH AB
AKE PERSSON
BOX 201
SE 151 23 SODERTALJE
SWEDEN

1 ISRAEL INST OF
TECHNOLOGY
S BODNER
FACULTY OF MECHANICAL
ENGR
HAIFA 3200
ISRAEL

1 DSTO
WEAPONS SYSTEMS DIVISION
N BURMAN RLLWS
SALISBURY
SOUTH AUSTRALIA 5108
AUSTRALIA

1 DEF RES ESTABLISHMENT
VALCARTIER
A DUPUIS
2459 BOULEVARD PIE XI NORTH
VALCARTIER QUEBEC
CANADA
PO BOX 8800 COURCELETTE
GOA IRO QUEBEC
CANADA

1 INSTITUT FRANCO ALLEMAND
DE RECHERCHES DE SAINT
LOUIS
DE M GIRAUD
5 RUE DU GENERAL
CASSAGNOU
BOITE POSTALE 34
F 68301 SAINT LOUIS CEDEX
FRANCE

1 ECOLE POLYTECH
J MANSON
DMX LTC
CH 1015 LAUSANNE
SWITZERLAND

NO. OF COPIES	ORGANIZATION
1	TNO DEFENSE RESEARCH R IJSSELSTEIN ACCOUNT DIRECTOR R&D ARMEE PO BOX 6006 2600 JA DELFT THE NETHERLANDS
2	FOA NATL DEFENSE RESEARCH ESTAB DIR DEPT OF WEAPONS & PROTECTION B JANZON R HOLMLIN S 172 90 STOCKHOLM SWEDEN
2	DEFENSE TECH & PROC AGENCY GROUND I CREWETHER GENERAL HERZOG HAUS 3602 THUN SWITZERLAND
1	MINISTRY OF DEFENCE RAFAEL ARMAMENT DEVELOPMENT AUTH M MAYSELESS PO BOX 2250 HAIFA 31021 ISRAEL
1	TNO DEFENSE RESEARCH I H PASMAN POSTBUS 6006 2600 JA DELFT THE NETHERLANDS
1	B HIRSCH TACHKEMONY ST 6 NETAMUA 42611 ISRAEL
1	DEUTSCHE AEROSPACE AG DYNAMICS SYSTEMS M HELD PO BOX 1340 D 86523 SCHROBENHAUSEN GERMANY

NO. OF
COPIES ORGANIZATION

2 COMMANDER
USA YPG
CSTE DTC YP MT EA
YUMA AZ 85365-9110

1 USAF AERONAUTICAL SYS CTR
ASC ENFC MR LEGER
WPAFB OH 45433-7809

1 COMMANDER
USA SBCCOM
AMSSC PM
NATICK MA 01760

4 COMMANDER
USA SBCCOM
AMSSB RAD D N
NATICK MA 01760

1 COMMANDER
USA SBCCOM
AMSSB RIM A N
NATICK MA 01760

1 COMMANDER
USA TRADOC
AAACO
ATCD SL
FT MONROE VA 23651-5194

1 COMMANDER
USA INFANTRY CTR & SCHL
ATZB CDC MR JONES
FT BENNING GA 31905

1 PRESIDENT
US ARMY OTC
AIRBORNE & SPEC OPS TST DIR
CSTE OTC AB
FT BRAGG NC 28310-0179

1 COMMANDER
US ARMY XVIII AIRBORNE CORPS
AFZA GF N MR COX
FT BRAGG NC 28307-5000

1 COMMANDER
US ARMY SPEC OPS COM
DSCLOG AOLO MA
MR MATHEWS
FT BRAGG NC 28307

NO. OF
COPIES ORGANIZATION

1 NVL UNDERSEA WARFARE CTR
TECH DEV & APPLCTNS GRP
P V CAVALLARO
CODE 74
1176 HOWELL ST
NEWPORT RI 02841

ABERDEEN PROVING GROUND

1 COMMANDER
USA DEV TEST CMD
CSTE DTC TT T MR JASTRAB
APG MD 21005-5055

INTENTIONALLY LEFT BLANK.

REPORT DOCUMENTATION PAGE			Form Approved OMB No. 0704-0188	
Public reporting burden for this collection of information is estimated to average 1 hour per response, including the time for reviewing instructions, searching existing data sources, gathering and maintaining the data needed, and completing and reviewing the collection of information. Send comments regarding this burden estimate or any other aspect of this collection of information, including suggestions for reducing this burden, to Washington Headquarters Services, Directorate for Information Operations and Reports, 1215 Jefferson Davis Highway, Suite 1204, Arlington, VA 22202-4302, and to the Office of Management and Budget, Paperwork Reduction Project(0704-0188), Washington, DC 20503.				
1. AGENCY USE ONLY (Leave blank)		2. REPORT DATE April 2002	3. REPORT TYPE AND DATES COVERED Final, May -November 2000	
4. TITLE AND SUBTITLE Evaluation of Static Line Webbing Materials Subjected to Simulated Airdrop Operating Conditions			5. FUNDING NUMBERS 622618H.80	
6. AUTHOR(S) Robert B. Dooley, Robert P. Kaste, James M. Sands, Gary W. Thibault,* and William L. Millette*				
7. PERFORMING ORGANIZATION NAME(S) AND ADDRESS(ES) U.S. Army Research Laboratory ATTN: AMSRL-WM-MB Aberdeen Proving Ground, MD 21005-5069			8. PERFORMING ORGANIZATION REPORT NUMBER ARL-TR-2713	
9. SPONSORING/MONITORING AGENCY NAMES(S) AND ADDRESS(ES) *U.S. Army Soldier Biological and Chemical Command Natick Soldier Center, Natick, MA 01760			10. SPONSORING/MONITORING AGENCY REPORT NUMBER	
11. SUPPLEMENTARY NOTES *U.S. Army Soldier Biological and Chemical Command, Natick Soldier Center, Natick, MA 01760				
12a. DISTRIBUTION/AVAILABILITY STATEMENT Approved for public release; distribution is unlimited.			12b. DISTRIBUTION CODE	
13. ABSTRACT (Maximum 200 words) An investigation was conducted to evaluate the mechanical performance of two types of static line webbing materials. Conventional Type VIII static line webbing and a proposed replacement, referred to as AbsorbEdge, were the primary subjects of the investigation. Tests were performed to evaluate the effect of each identified and simulated airdrop operating condition. Test methods used in the investigation included straight and 90° bend tensile tests to evaluate the effects of straining over a series of specified bend radii. Additional tests were performed to investigate the effect of textured bend surfaces, the number of twists in a line between test grips, the effect of retained water in the line, the effect of mechanical fatigue, and the effect of various cotton and polymer-based textile sheaths located at the bend fixture/specimen interface. Results from these and other tests are contrasted against the results of straight-pull tests to evaluate the adverse effect of the test variables on the baseline strength of each material. A theory regarding how the line construction distributes tensile loads around a door edge and decays line system strength is presented. Test results are used to compliment failure observations and are presented within this report.				
14. SUBJECT TERMS static line, Type VIII static line, AbsorbEdge			15. NUMBER OF PAGES 86	
			16. PRICE CODE	
17. SECURITY CLASSIFICATION OF REPORT UNCLASSIFIED	18. SECURITY CLASSIFICATION OF THIS PAGE UNCLASSIFIED	19. SECURITY CLASSIFICATION OF ABSTRACT UNCLASSIFIED	20. LIMITATION OF ABSTRACT UL	

INTENTIONALLY LEFT BLANK.